Supporting Information

AI-assisted exploration of superionic glass-type Li^+ conductors with aromatic structures

Kan Hatakeyama-Sato, Toshiki Tezuka, Momoka Umeki, and Kenichi Oyaizu*

*oyaizu@waseda.jp

Index

The latest database for Li^+ conductors and source code to process the database can be obtained from the corresponding author upon request. Database is also available on our website (http://www.appchem.waseda.ac.jp/~polymer/PolymerDatabase/)

Preparation of Li^+ conductor database

The database for Li^+ conducting polymers and monomeric species was prepared by manually collecting related information from about 250 scientific publications (journal articles, books, and research reports, not patents) using reviews,[1-6] search engines, and a polymer database (PolyInfo: https://polymer.nims.go.jp). All data were collected and checked manually by Ph.D. researchers and graduate students (in the authors' group) specializing in functional polymers. The database covered most basic chemical structures for polymeric and monomeric Li^+ conductors reported up to 2018 (>2000 types of composites and about 400 chemicals, Figures S1 and S2). Properties of the conductors, such as chemical structure, composition ratio, temperature, and conductivity, were inputted into the database. Chemical structures were recorded according to simplified molecular-input line-entry system (SMILES). Recently, an extended system of SMILES was reported to describe the information on polymers more accurately (BigSMILES).[7] However, we utilized the normal SMILES format because there was still no available Python library to process the new format. For lithium salts, only their anion structures were inputted (*e.g.*, ClO_4^- for lithium perchlorate). In the cases of macromolecules, their molecular weight, copolymerization ratio, and polymer structures (*e.g.*, block, random, cross-linked, etc.) were recorded in the database. Due to the insufficient structure information, grafting polymers connected to inorganic additives were not included. Some polymers, such as those containing electrochemically unstable groups for batteries (*e.g.*, allyl and hydroxyl)[8] or structures too similar to the already inputted ones (*e.g.*, a slight increase of alkyl chain),[8] were not inputted. Those polymers will be recorded in the future database. Representative conductors reported in early 2019, whose structures and composition were described clearly,[9-16] were inputted into the database, but used only for prediction.

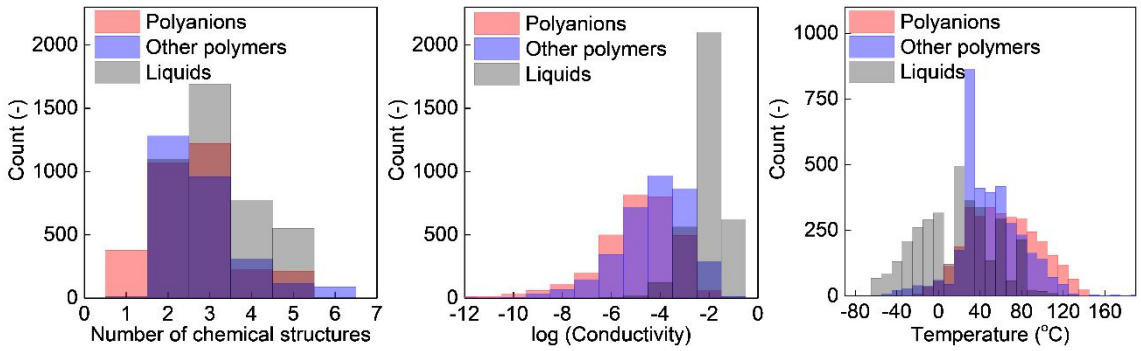

(a) (b) (c)

Figure S1. Histograms showing information about the training database (*i.e.*, inputted conductors reported by 2018). (a) Number of chemical structures in included one conductor. (b) Ionic conductivity. (c) Measured temperature. The word 'Liquids' in the legend refers to liquid electrolytes.

Polyanions

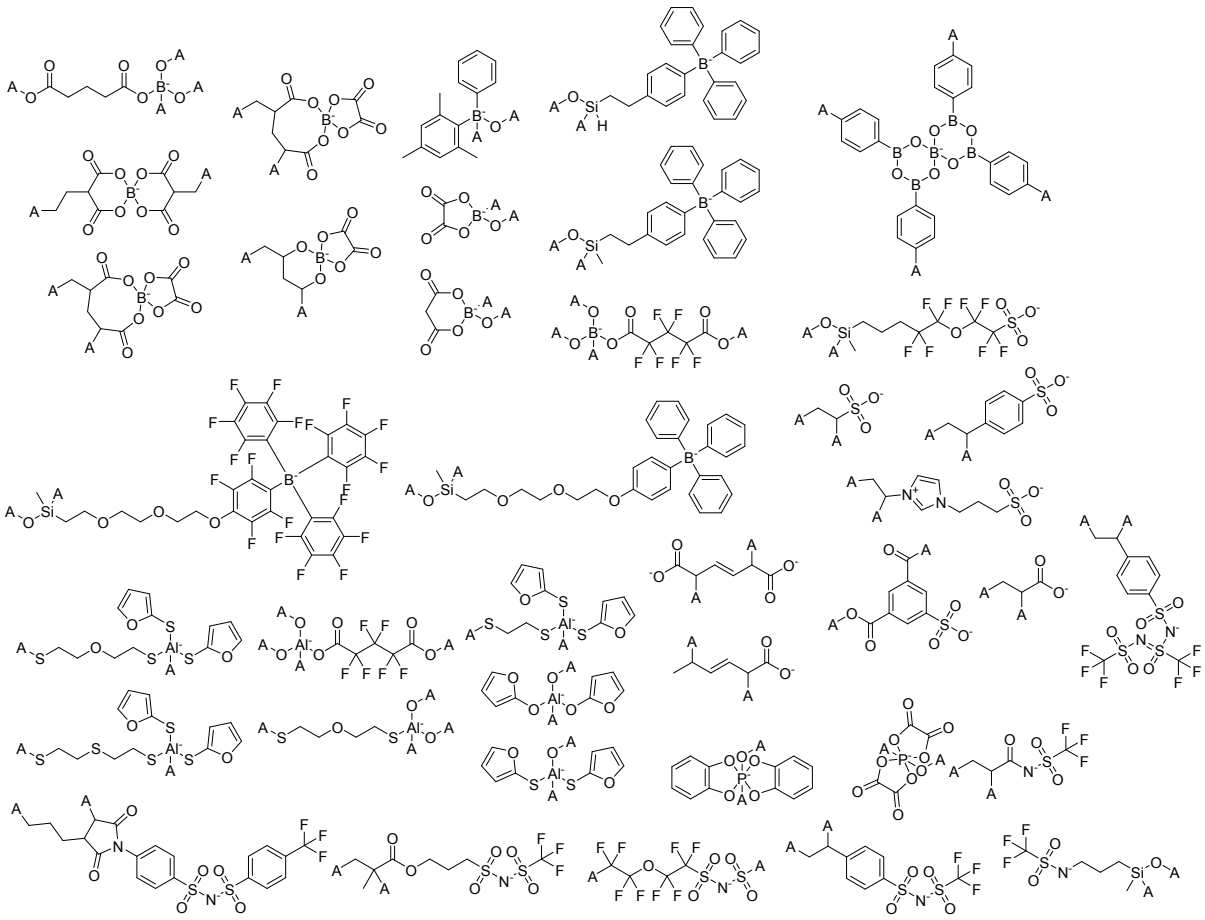

Anions

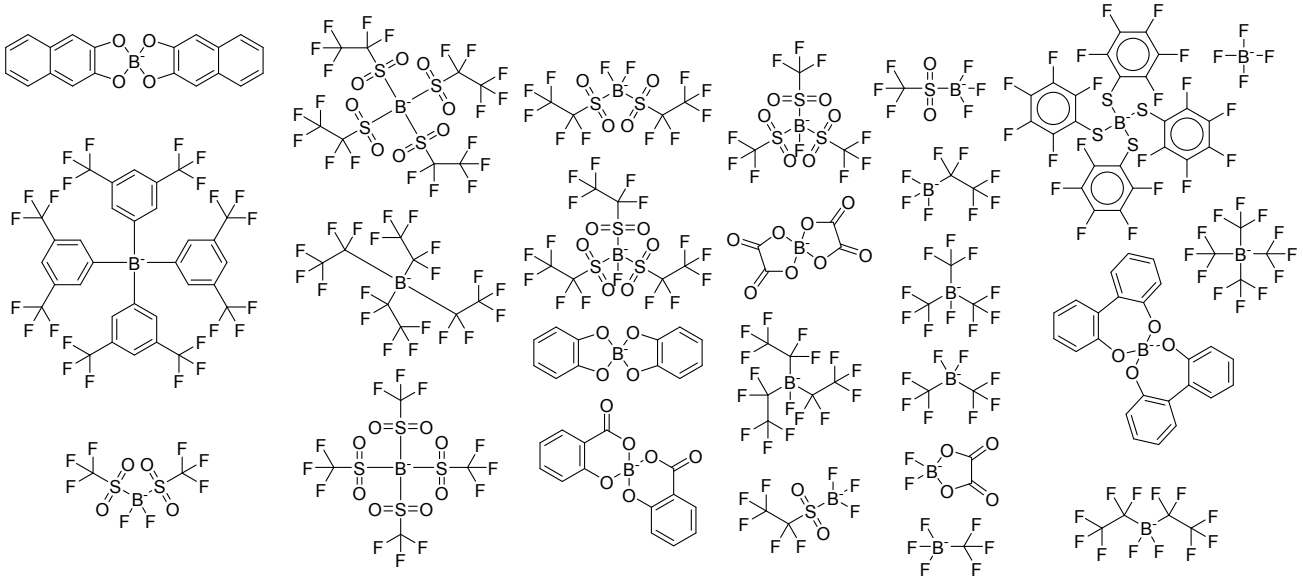

(continued from the previous page)

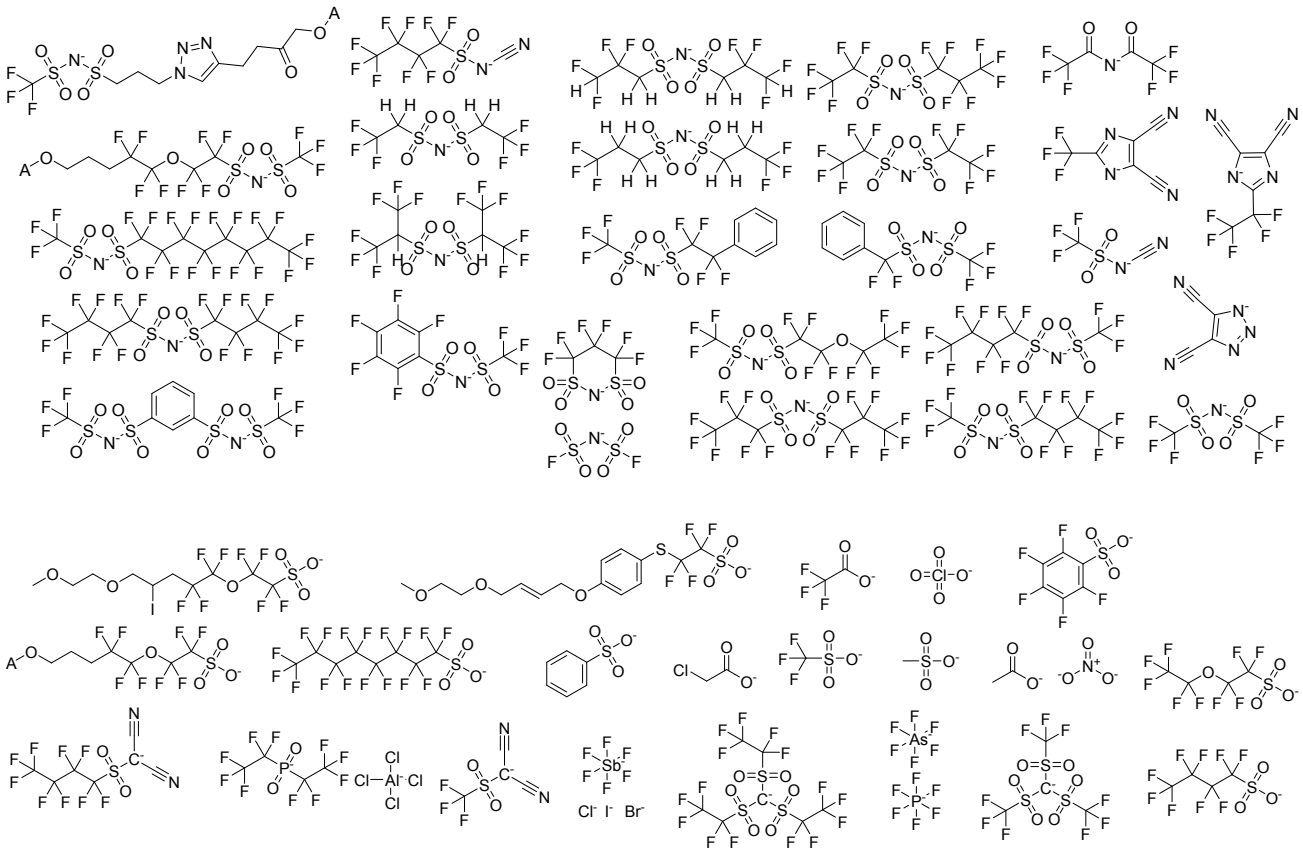

Neutral polymers

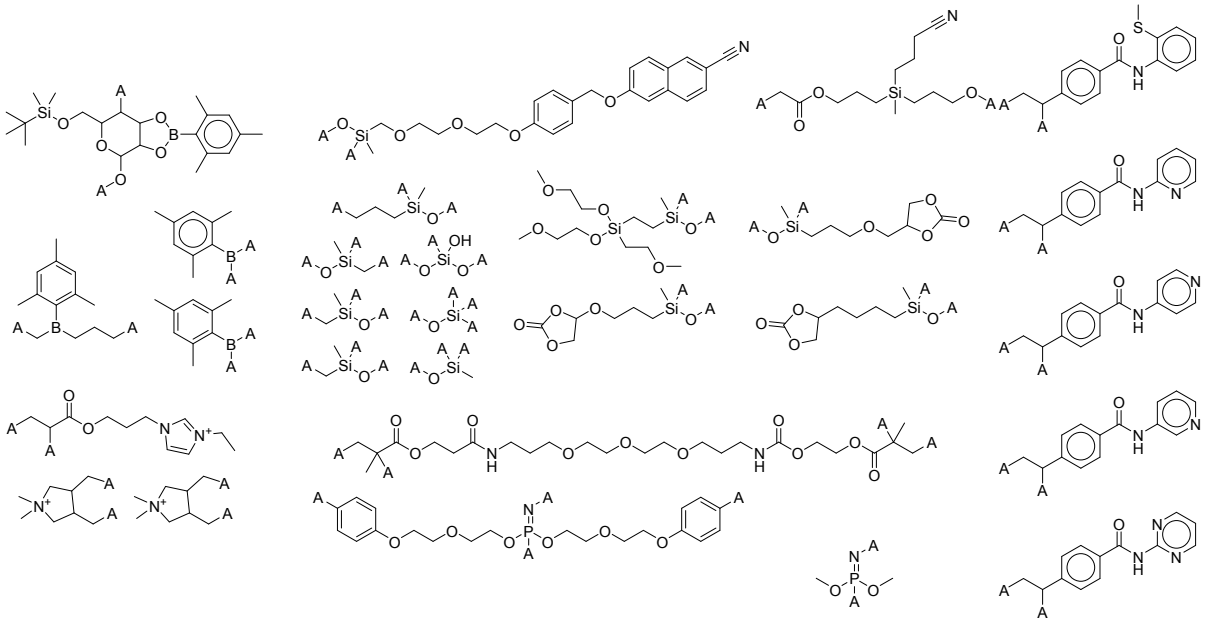

(continued from the previous page)

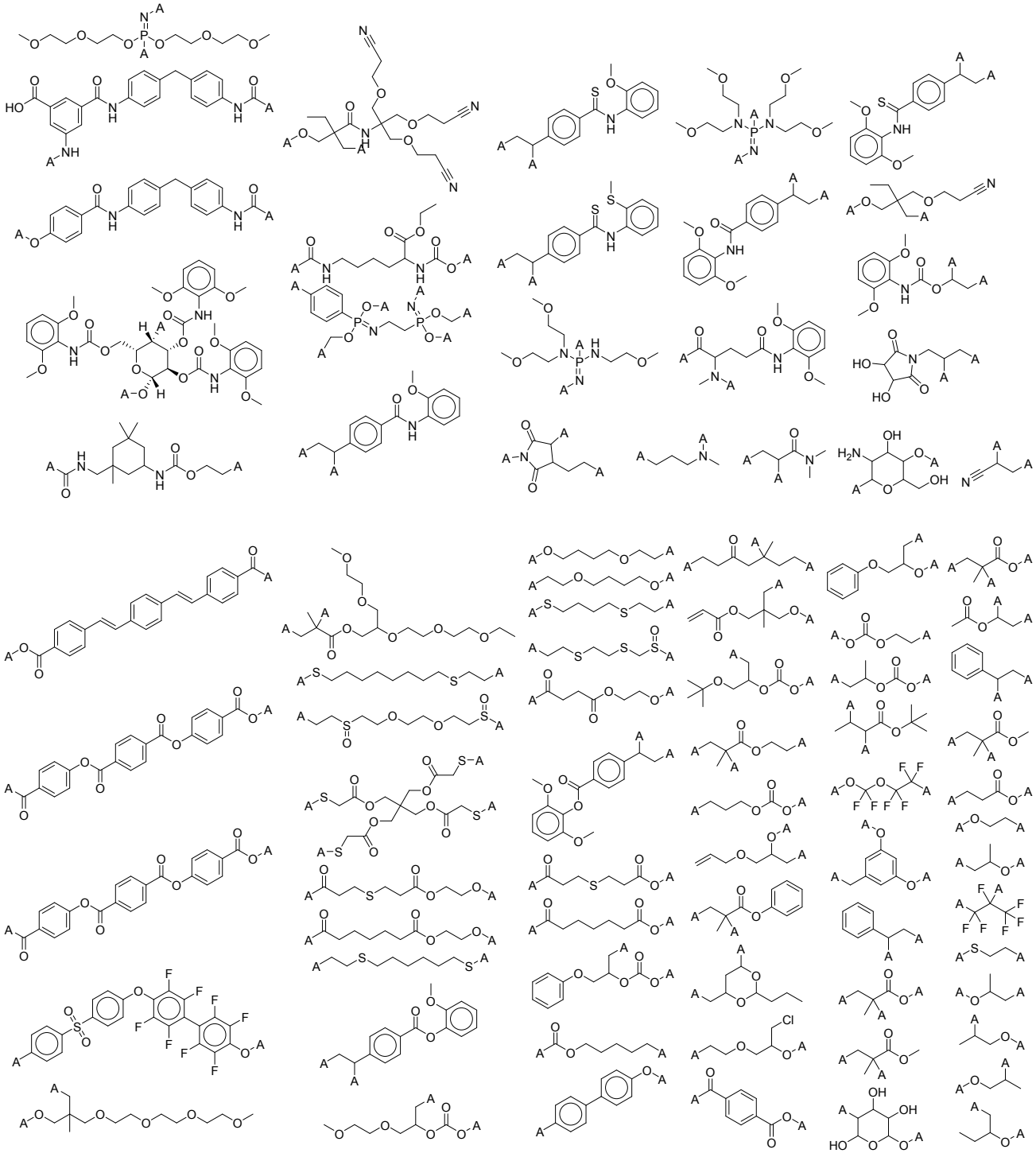

(continued from the previous page)

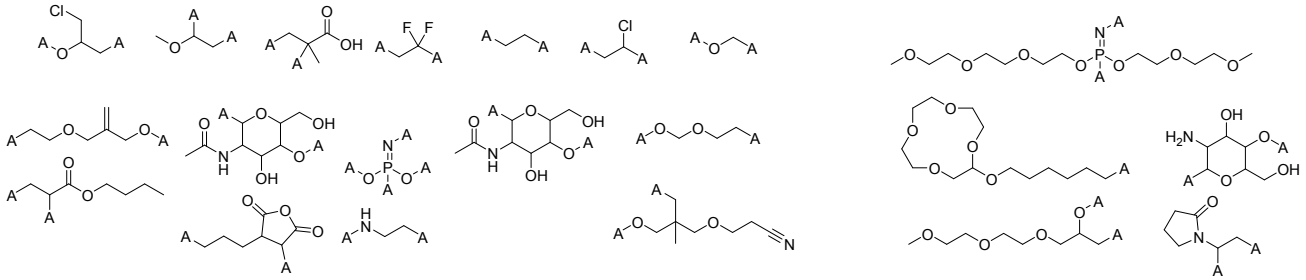

Solvents/plasticizers/others

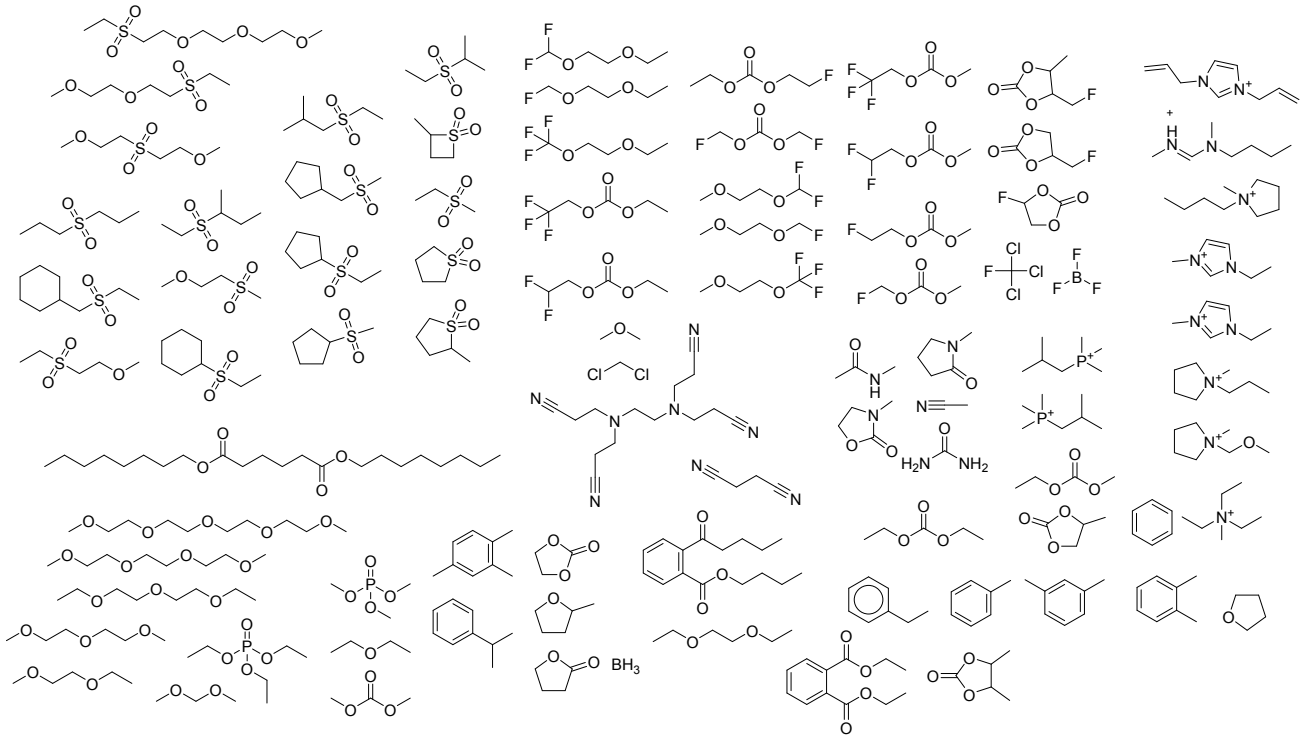

Figure S2. Typical chemical structures included in the database. ‘A’ indicates that a structure is connected to the other chemicals (*i.e.*, polymers and/or grafting units).

Summary of machine learning

In this section, the overview of machine learning is summarized. The detailed methods are described in the later sections.

(1) Conversion of the database for machine learning

All inputted information was converted to numeric vectors, using an original Python 3.6 scripts to conduct machine learning (Figures S3 and S4). Conductivity was used in a logarithmic scale because the parameter had a wide range of values (10^{-14} to 10^{-1} S/cm). The types of the inorganic additives (*e.g.*, SiO_2, Al_2O_3) and polymer structures (*e.g.*, copolymer, branched) were inputted as character strings, but automatically converted to one-hot vectors. Chemical structures were transformed to the arrays of floating-point numbers (*vide infra*).

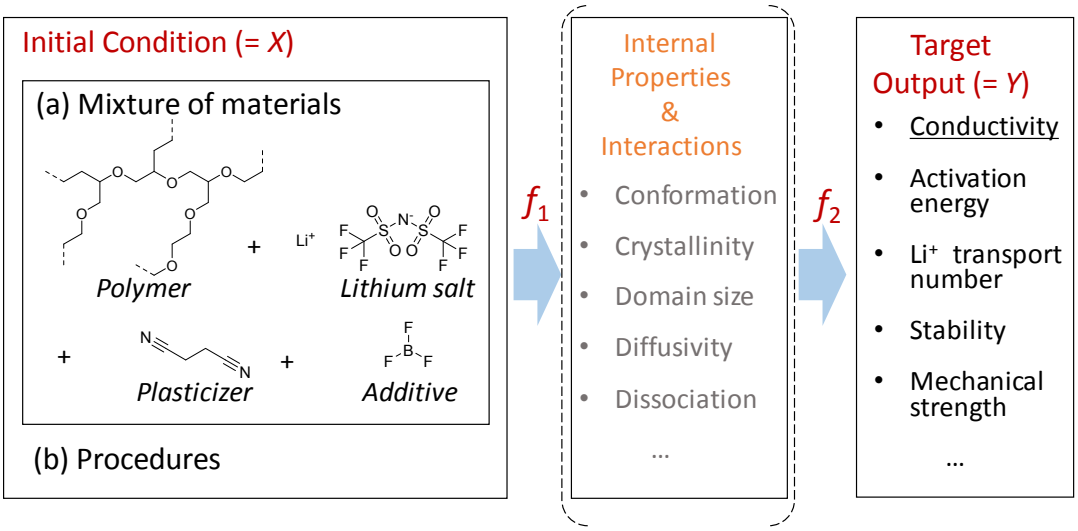

Figure S3. Relationship between the inputted condition (X), internal properties, and output properties (Y) for the Li^+-conducting polymer composites. The final output can be expressed as $Y = f_2(f_1(X))$. In this study, ionic conductivity was selected as Y, and effects of procedures were ignored.

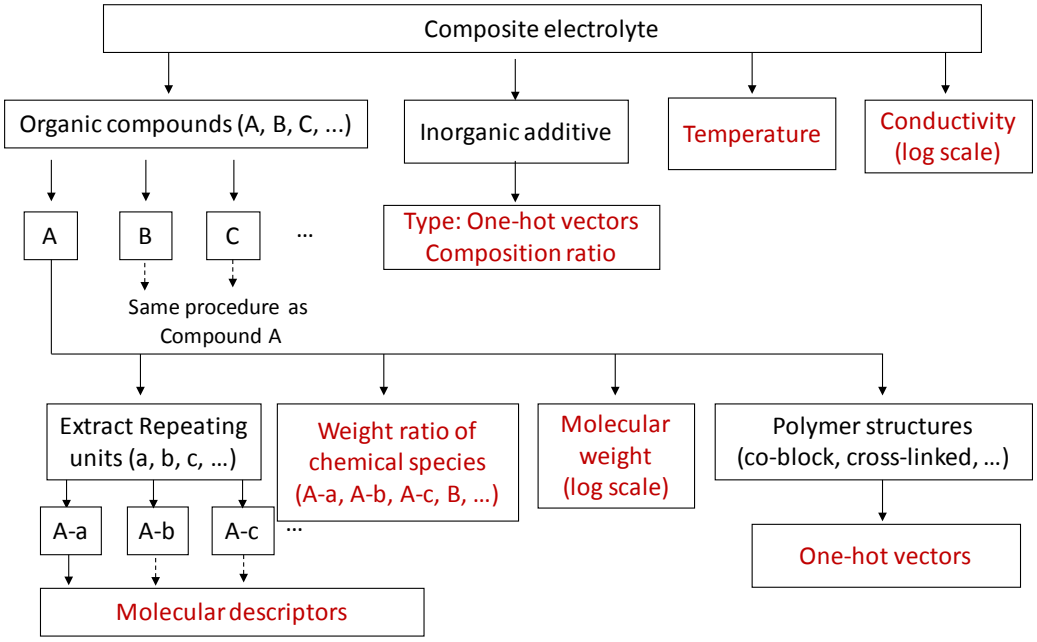

Figure S4. Overview of converting the inputted information to numeric vectors. Vectorized data are highlighted in red.

(2) Graph neural network to recognize molecules

Currently, there is no standard way of expressing polymer structures with numeric vectors. Using Mordred package, which automatically calculates about 2000 descriptors per chemical structure,[17] was found to be effective to describe the chemical features precisely.[9] However, the dimension of the vectors for one conductor, consisting of typically three chemical species (*i.e.*, about 6000 descriptors per conductor), may be too large to finish the training of Gaussian process within a practical time. Here, the characteristics of the inputted molecules were expressed by 32-dimensional vectors using a pretrained gated graph neural network (GGNN; Figure S5). Initially, the GGNN was connected to a two-layer perceptron with about 2000 output units. The relationship between the structures and their 2000 chemical properties were trained with the *in-silico* compound database (Figure S6). The *in-silico* database (*vide infra*) was important because the number of chemical structures in the main database (about 400) might be insufficient to train the neural network ($>10^4$ samples are normally required).[18] The pretrained neural network could recognize a variety of chemical structures and express them with the 32-dimensional vectors, which were correlated with the 2000 general chemical properties (Figure S7). The output of the model was passed to Gaussian process for the conductivity prediction.

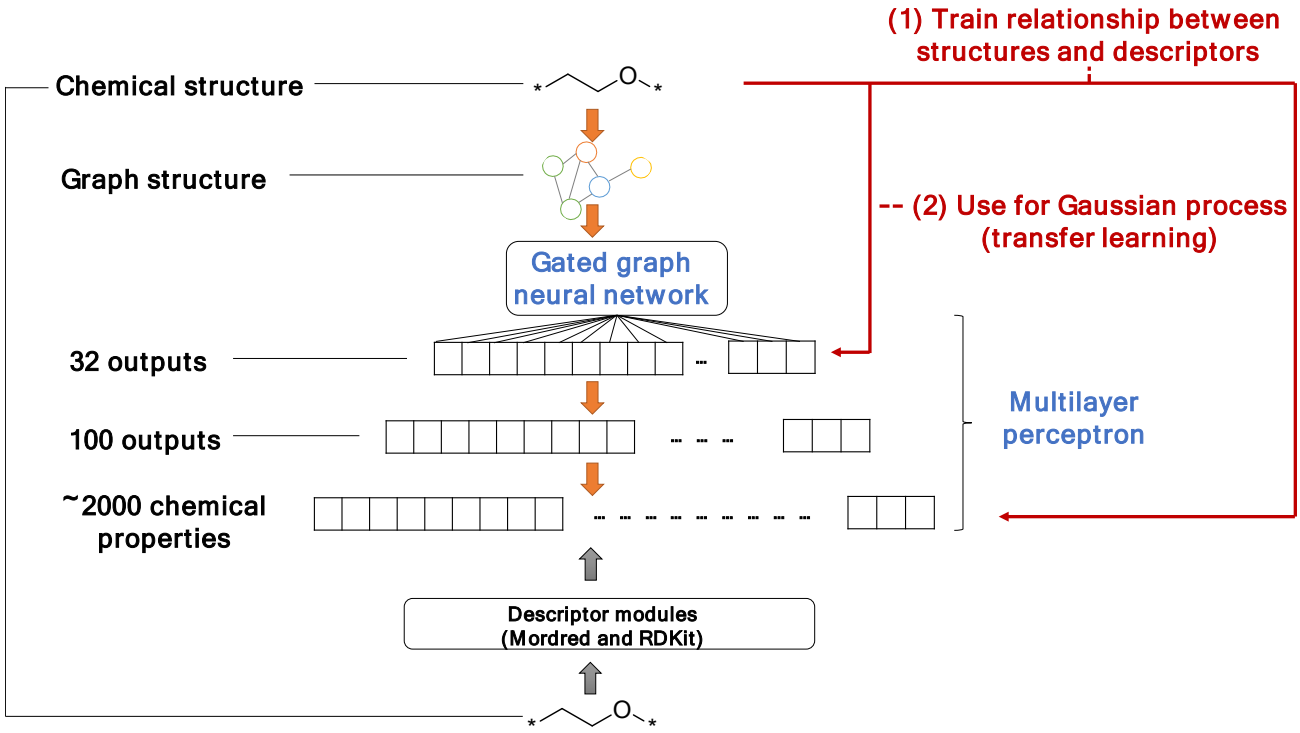

Figure S5. Procedures for transfer learning to express molecular features. Initially, a database containing chemical structures and their 2000 molecular descriptors was prepared. The relationship between the chemical structures and their descriptors was trained by a stacking model of the GGNN and MLP. Then, the 32-dimensional vectors, the output of the trained GGNN, were used for the main machine learning purpose.

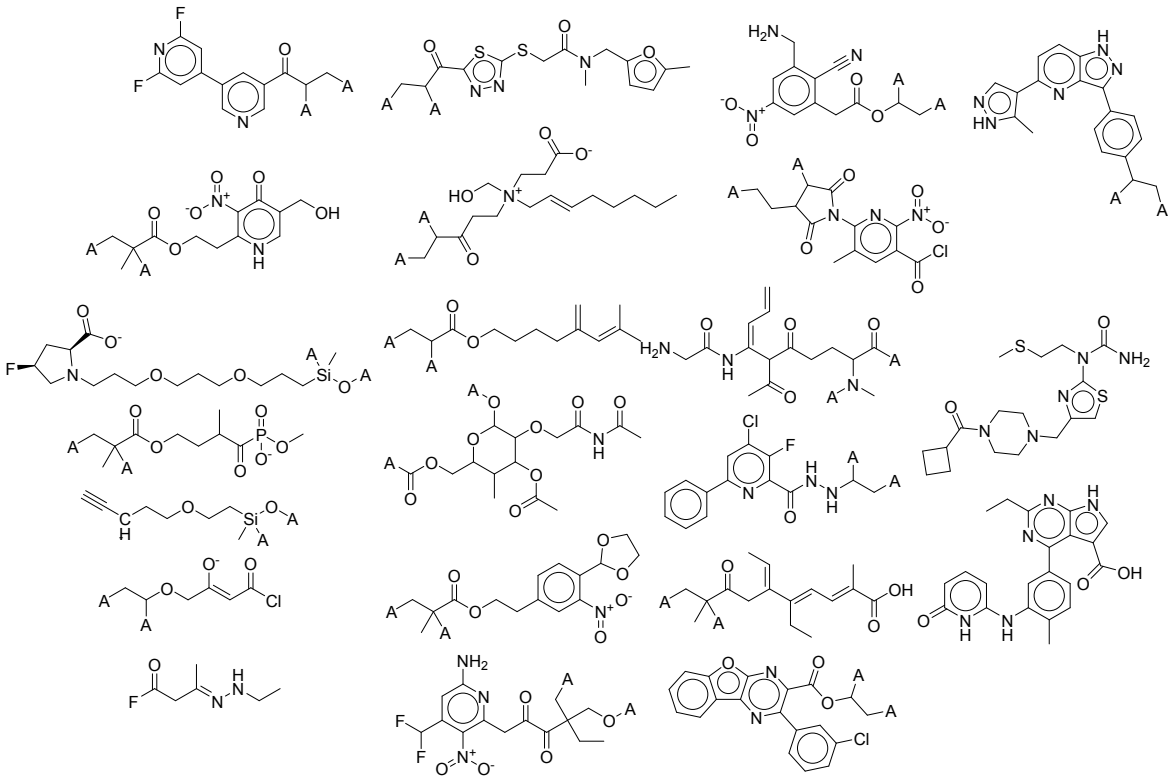

Figure S6. Example structures of randomly generated compounds, which were used for transfer learning.

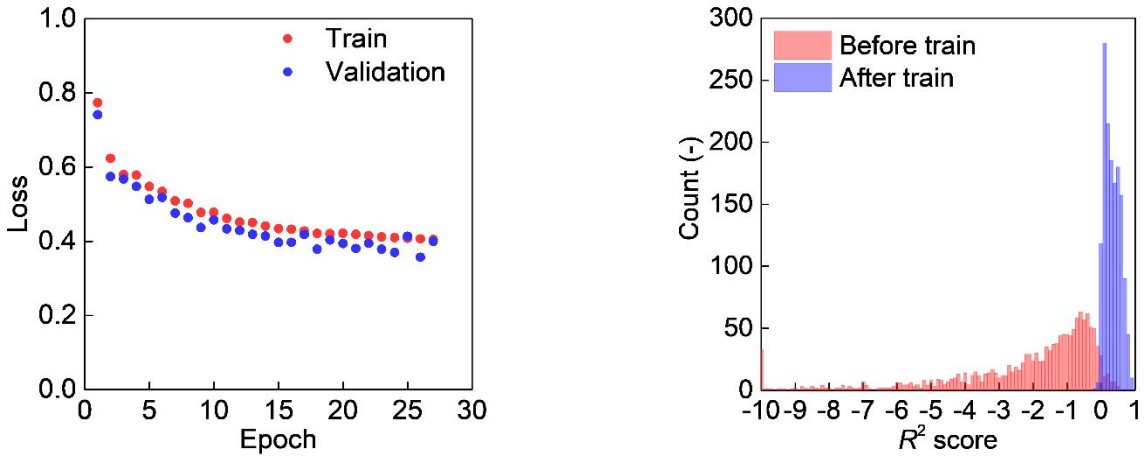

(a) (b)

Figure S7. Pretraining results for the GGNN. (a) Learning process of the neural network. The network was trained with the randomly generated compound database. (b) Distribution of R^2 scores for each actual and predicted descriptor value before and after training.

(3) Preparation of the *in-silico* compound database

To pretrain the GGNN, a new database of randomly generated organic polymers and monomeric species was prepared because the previously reported quantum chemistry databases focused on only monomeric species with limited elements (H, C, N, O, and S).[19-20] First, conventional organic compounds were collected from ZINC (http://zinc.docking.org), PubChem (https://pubchem.ncbi.nlm.nih.gov), and this database. The chemicals were fragmented and reconnected randomly to yield about 5×10^4 random polymers and monomeric species (example structures are shown in Figure S6). Their chemical features (molecular descriptors) were calculated by the Mordred[17] and RDKit (https://www.rdkit.org) modules.

(4) Predicting conductivity with machine learning models

In Figure 2a, all samples reported by 2018 were used for training, and samples in 2019 were used for testing. For comparison with the GGNN, multilayer perceptron (MLP), Lasso regression, principal component analysis (PCA), and uniform manifold approximation and projection (UMAP)[21] techniques were examined as the dimension reduction approaches, using the training dataset (Figure S8).

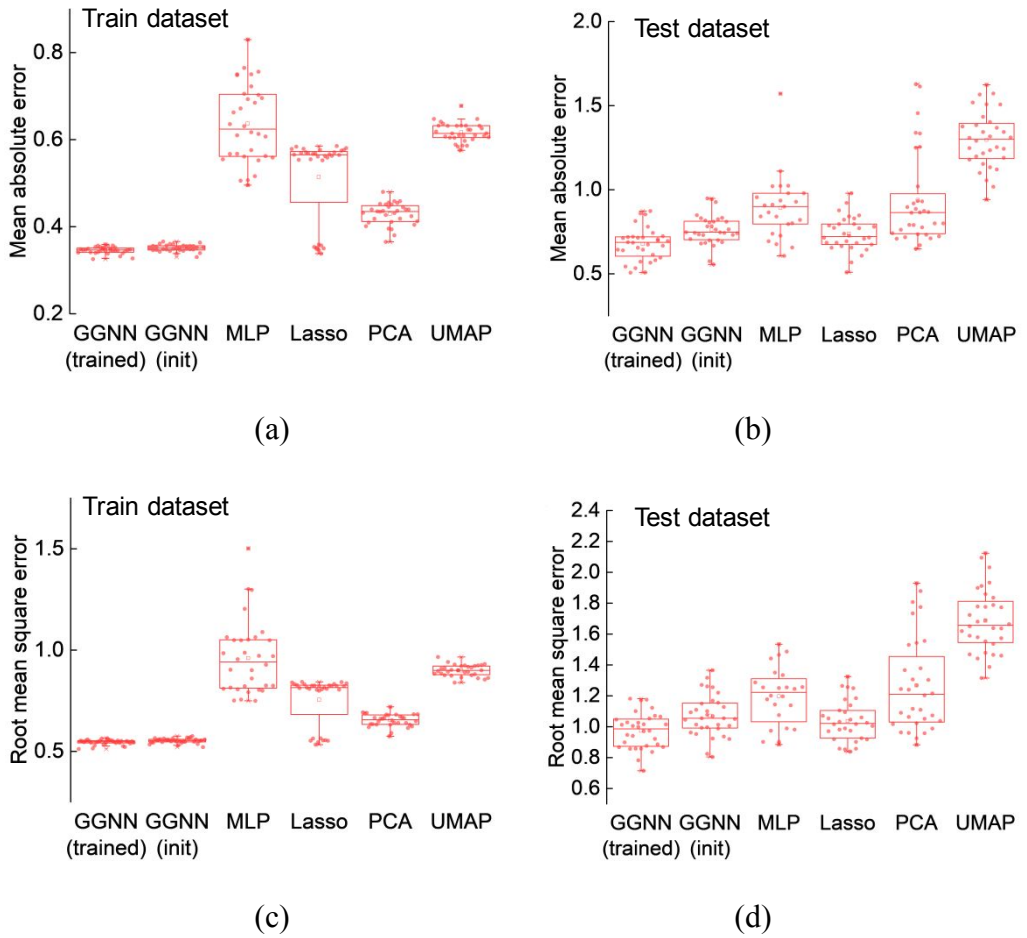

Figure S8. Comparison of dimension reduction approaches by box plots. (a) and (b) Mean absolute error of experimental and predicted conductivity for training and test datasets. (c) and (d) Root mean square error. For comparison, several different models/approaches were used to show the

superiority of the pretrained GGNN. The GGNN before pretraining (initial state) gave larger errors owing to the lack of the molecular recognition capability. A larger variance of error was obtained by the MLP (with three hidden layers, sizes of 1000, 500, and 100), due to its inferior recognition of chemical structures. A linear model, Lasso regression, was not preferred to express the complex interactions of the polymer composites, as indicated by the larger errors and variances for the training dataset. Conventional dimension reduction techniques, PCA and UMAP (an improved model of t-distributed stochastic neighbor embedding, t-SNE),[21] could not extract and express the essential chemical features accurately.

Detailed format of the database

The constructed database consists of 1) compound and 2) composite subparts. The compound database includes the basic information for the polymers and monomeric species used for the conductors. In the composite database, the properties of the electrolytes, as the mixtures of the chemicals in the compound database, are recorded.

(1) Compound database

In the compound database, the properties of organic compounds, including polymers, were recorded by numbers and character strings. Figure S9 shows the example schemes to convert the original chemical information to be recordable in the database. For instance, a brush type polymer consisting of polyphosphazene and PEO side chains (nickname: GraftPolymer1) is shown. First, the repeating units of the polymers were extracted. To clarify the repeating parts, the chemical bonds connected to the other repeating units were marked by Mg atoms. Magnesium was selected simply because it did not appear in any chemicals in the compound database. Similarly, the grafting

bonds were capped by Ca atoms. All repeating units were fragmented and capped by Mg or Ca symbols.

The fragmented chemicals, polyphosphazene and PEO units, were expressed by SMILES ([Mg]N=P(O[Ca])(O[Ca])[Mg] and [Mg]CCO[Mg], respectively). Their character strings were joined by period ([Mg]N=P(O[Ca])(O[Ca])[Mg].[Mg]CCO[Mg]). Then, the equivalent ratio of the two chemical units was calculated. Here, $5 \times 2 = 10$ equivalents of PEO units were available against phosphazene. Therefore, the molar ratio "1/10" was inputted in the database. Some original reports used weight ratios instead of mole to describe chemical compositions. In such cases, weight ratio was used, for easiness and to avoid calculation errors.

The types of polymer structures were recorded as character strings, such as "graft", "block", and "normal" (nothing inputted for "normal" structures). Molecular weights (M_n, M_w, M_w/M_n, and/or polymerization degree) were also recorded. Crystallinity, melting point, and glass transition temperature were inputted with some cases. However, they were not inputted in most cases because of the lack of available data in the literature, and the limited time to construct the database. These three parameters were not used for machine learning in the current study.

Another component, LiTFSI (nickname: LiTFSI), was also inputted to the database. Li^+ was removed from the structure, because the cation was rather redundant (*i.e.*, this study focuses on only Li^+ conductors). The SMILES expression of the anion (FC(F)(F)S([N-]S(=O)(C(F)(F)F)=O)(=O)=O) was recorded. For monomeric species such as LiTFSI, their polymerization degree and M_w/M_n were inputted as 1.

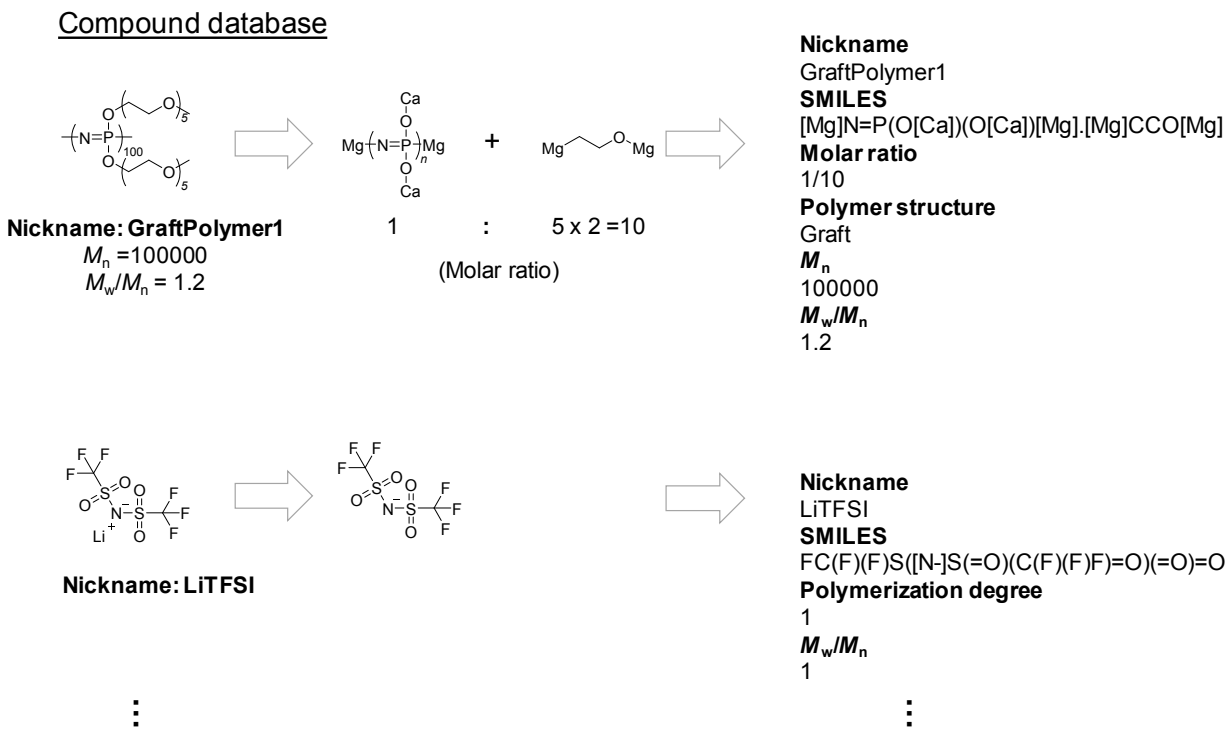

Figure S9. Format of the compound database.

We note that some information, described below, were ignored and/or simplified during the conversion. Still, the simplifications could be justified in the viewpoints of the reasonably high prediction accuracy achieved in this study, the cost of collecting the additional information, and the lack of the available experimental data in the original reports.

[Representative ignored/simplified factors]

a) End group of the polymers

(*e.g.*, the end group of PEO is normally -OH, while functional groups such as -CH_3 are introduced in some cases)

b) Detailed information on higher order polymer structures

(*e.g.*, quantitative parameters such as fractal dimension can be employed for branched polymers, but no available data reported in most cases)

c) Physical properties such as crystallinity and melting point

d) Processing and/or hysteresis information

e) Bonds for repeating units

(*i.e.*, capped by Mg or Ca in this study)

f) Connections and interactions with inorganic materials

(grafted polymers to inorganic materials were not recorded in the database)

g) Order of repeating units in block polymers

(*e.g.*, poly(A-*b*-B-*b*-C) and poly(A-*b*-C-*b*-B) would be regarded as the same polymer because the database considered only the equivalent ratio of the repeating units)

h) Detailed grafting/copolymer information

(*e.g.*, GraftPolymer1 has two ethylene glycol units with $n = 5$. On the other hand, a graft polymer having the different side chain lengths, such as $n = 3$ and 7, respectively, would be recorded as the same polymer, because the database considers only the equivalent ratio of the repeating units)

i) Reliability of the original report

As the specialists of functional polymers and organic electrochemistry, we checked the experimental data of all inputted cases. Some samples, giving unnatural responses (*e.g.,* too large/small conductivity compared to other similar samples), were removed. However, additional conductivity measurements were not conducted to validate the reliability of the results.

(2) Composite database

The composite database stored the properties of the electrolytes consisting of the chemicals recorded in the compound database. An example composite of GraftPolymer1 and LiTFSI is shown in Figure S10. The electrolyte was prepared with a composition of [O]/[Li] = 12/1, where [O] was the number of oxygen atoms in a repeating unit of the polymer. 15 wt% of SiO_2 particles were also mixed as the additive. In that case, the mixture was recorded as "GraftPolymer1/LiTFSI" with a molar ratio of "1/1" (*i.e.*, 12 oxygen atoms available in the polymer unit). The type of inorganic additive was inputted as a word, "SiO_2", and its weight ratio was inputted as a number, "15" wt%. Measured temperature and ionic conductivity were also recorded as numbers. The numbers were read from the tables and/or figures in the original reports manually. WebPlotDigitizer (https://automeris.io/WebPlotDigitizer/), a web-based tool to extract data from images, was used to read data from graphs. Ionic conductivity was recorded by AC impedance with the most cases and by DC current with some cases. However, for convenience, we did not distinguish the cases. Physical properties of the composites, such as crystallinity, melting point, and glass transition temperature were recorded with some cases. However, they were not used for machine learning on the basis of the same reason as the compound information.

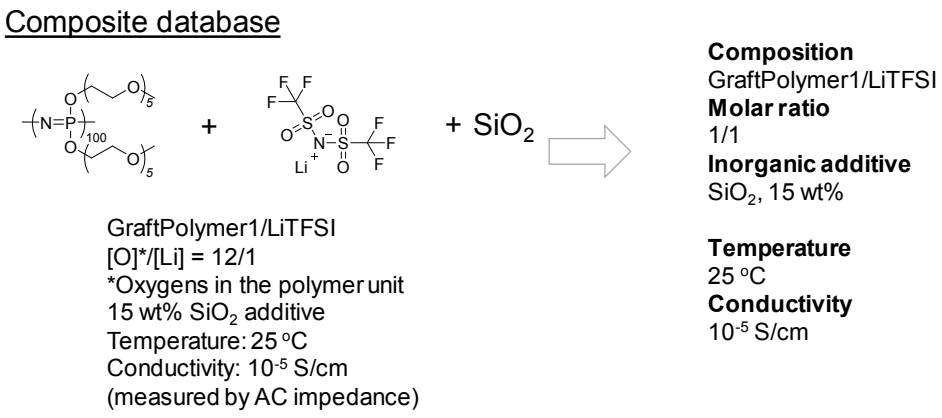

Figure S10. Format of the composite database.

As explained above, the database was constructed based on simplifications. However, it should be emphasized again that the high accuracy prediction achieved in Figure 2 supported the validity of the database for machine learning. In other words, the inputted data covered the most essential information for the prediction of ionic conductivity. The additional input of experimental properties would somewhat increase the accuracy. However, the preparation of the complete, ideal dataset may not be feasible in the viewpoints of a huge cost and time.

Preprocessing the database for machine learning

This section explains the way to convert the database for machine learning, using an example composite of "GraftPolymer1/LiTFSI = 1/1 (mol/mol) + 15 wt% SiO_2" (Figure S11).

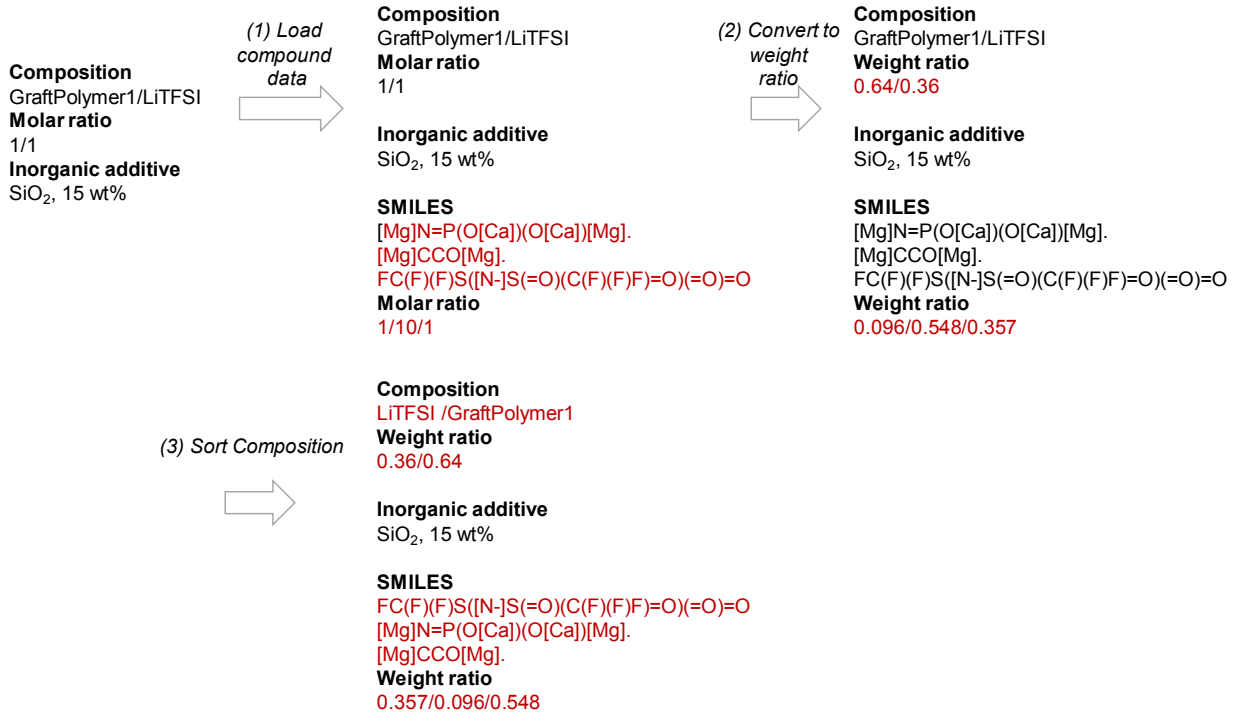

Figure S11. Processing the composition data for machine learning (part 1).

(1) Load compound data

By referencing the compound database, SMILES strings and molar ratio of the consisting chemicals were loaded. SMILES strings of the chemicals were joined by period. The data consists of two main parts: a) "composition" (GraftPolymer1/LiTFSI) and b) "SMILES" ([Mg]N=P(O[Ca])(O[Ca])[Mg].[Mg]CCO[Mg].FC(F)(F)S([N-]S(=O)(C(F)(F)F)=O)(=O)=O)).

(2, 3) Convert to weight ratio

Molecular weights of all chemicals expressed by SMILES (ignoring Mg and Ca atoms) were calculated. Then, the weight ratio of each component and SMILES was calculated. Orders of the compounds and SMILES were sorted by their charges so that anions (*e.g.*, $TFSI^-$) appear in the first position.

(4) Load compound data

From the compound database, structure types of the compounds (*e.g.*, "graft", "block", and "normal") and Log(M_w) were loaded. Polydispersity or M_n was not used for machine learning. If M_w was not reported, M_n was used instead. If no information on molecular weights was recorded, the median of M_w in the database was used (Figure S12).

(5) Fill missing values

For machine learning, 6 types of compounds and SMILES could be inputted in maximum. If the numbers were less than 6, the "blank" components or SMILES, having a weight ratio of 0, a structure of "normal", and Log(M_w) of 0 were inputted.

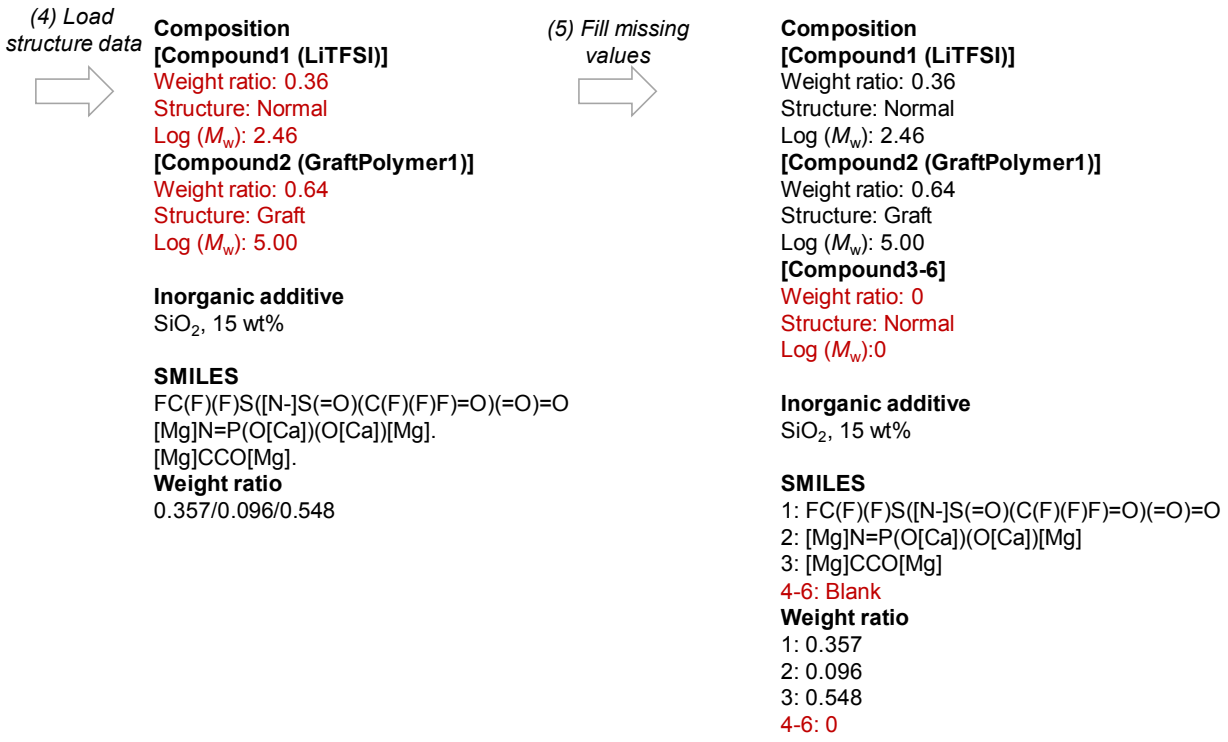

Figure S12. Processing the composition data for machine learning (part 2).

(6) Vectorization

To convert all information to numbers, the types of compounds and inorganic additives, and SMILES strings were converted to vectors according to the following rules.

[Structure types of compounds]

The inputted character strings (graft, normal, etc.) were converted to, namely, one-hot vectors. Firstly, all structure types except for “normal” were simplified to be “copolymer”. This approximation was done because the database (or the original literature) did not contain satisfactory information for machine learning in the viewpoints of both quantity and quality. Then, the words, “normal” and “copolymer”, were converted to the corresponding vectors, (1, 0) and (0, 1), respectively.

[Inorganic additives]

The types of inorganic additives were treated in a similar way to the structures of the compounds. For simplicity, the additives were classified into three types a) "blank" (no additive), b) "MO_x" (simple metal oxides such as SiO_2, TiO_2, and Al_2O_3), and c) "others". The character strings were converted to the vectors, (1, 0, 0), (0, 1, 0), or (0, 0, 1), respectively.

[SMILES]

Chemical structures recorded as SMILES were inputted to a machine learning model, gated graph neural network (GGNN) as graph structures (*vide infra*). The model could recognize their chemical features, and calculate the corresponding 32-dimensional vectors. For instance, a SMILES string "FC(F)(F)S([N-]S(=O)(C(F)(F)F)=O)(=O)=O" was converted to a 32-dimensional vector, (-1.25, 0.88, ..., -3.08) in Figure S12. "Blank" SMILES was converted to a zero vector (0, 0, …, 0).

All related information was converted to numbers by this step (*i.e.*, floating-point numbers in Python).

(7, 8) Extracting numbers and standardization

All numbers were concatenated as one vector, having a dimension of *ca.* 200. All parameters except for one-hot vectors were converted to z-scores for standardization (test datasets were standardized using the mean values and standard deviations of the training dataset).

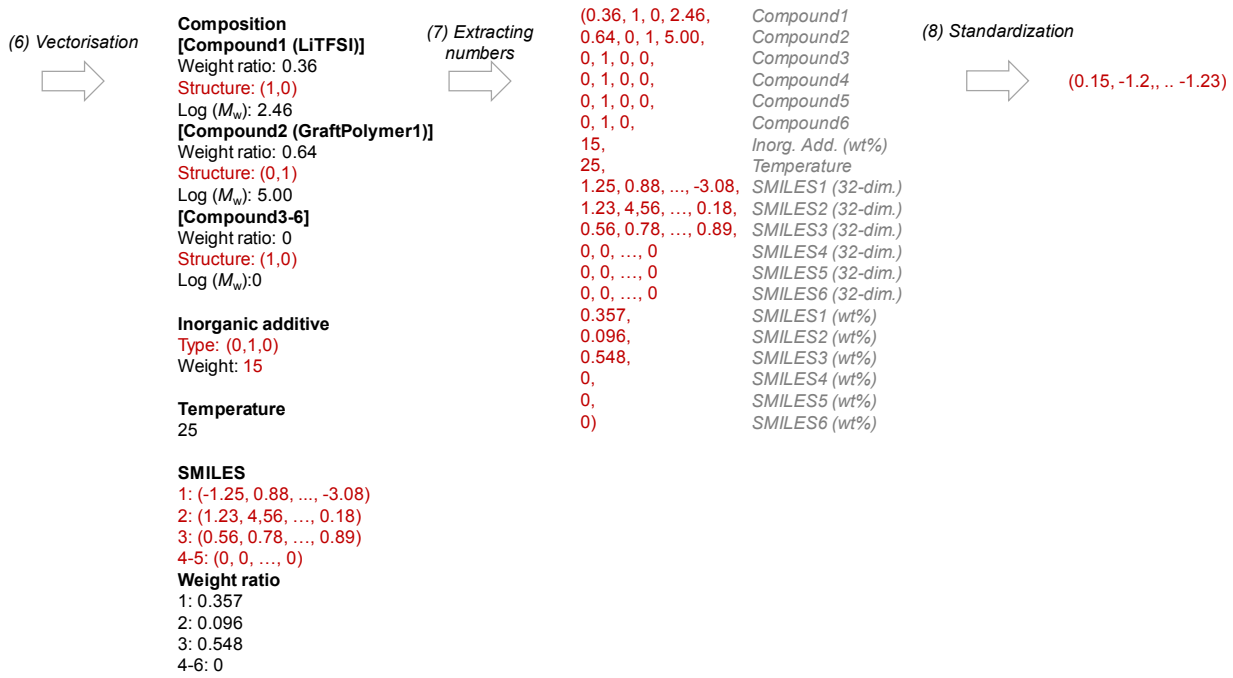

Figure S13. Processing composition data for machine learning (part 3).

Machine learning of ionic conductivity

The relationship between the electrolyte information (X), prepared in the previous section, and logarithmic ionic conductivity (y, standardized as z-score) was approximated using a nonlinear function, Gaussian process, f_{GP} (Figure S14). The inputted X contained the information including weight ratio, molecular weight, characteristic vectors of SMILES, and measured temperature. As a kernel function, a hyperparameter of Gaussian process, Matern 3/2 was selected. Noise components were not included in the kernel because it did not improve the prediction accuracy.

As the control experiments, *ca.* 2000 molecular descriptors (per a chemical structure) were used instead of the 32-dimensional vectors generated by the GGNN. The prepared input, X (> 10000-dimensional vector) was directly passed to MLP or Lasso models. Another approach was to compress the vectors preliminarily by PCA or UMAP algorithms. The compressed 200-dimensional vectors were inputted to Gaussian process. Implemented functions of an open-source module, Scikit-learn 0.20.2, were used for Gaussian process, MLP, Lasso, and PCA. Detailed

information is described on the website (https://scikit-learn.org/). For UMAP, an open-source library, umap-learn 0.3.10, was used.

For the model comparison, 8-hold cross validation was conducted (Figure S8). The database up to 2018 was split into training and test datasets. The conductors were divided into training and test datasets randomly. For instance, the composites of A/B/C = 1/1/1 (wt/wt/wt) and A/B/C = 1/1/2 were considered as the same conductor, and always kept in the same group. On the other hand, the pair A/B/C and D/B/C were considered as different conductors, and could be divided into different datasets randomly (A, B, C, and D represent different chemical structures). The cross validation was repeated four times because the prediction results changed slightly because of the random splitting.

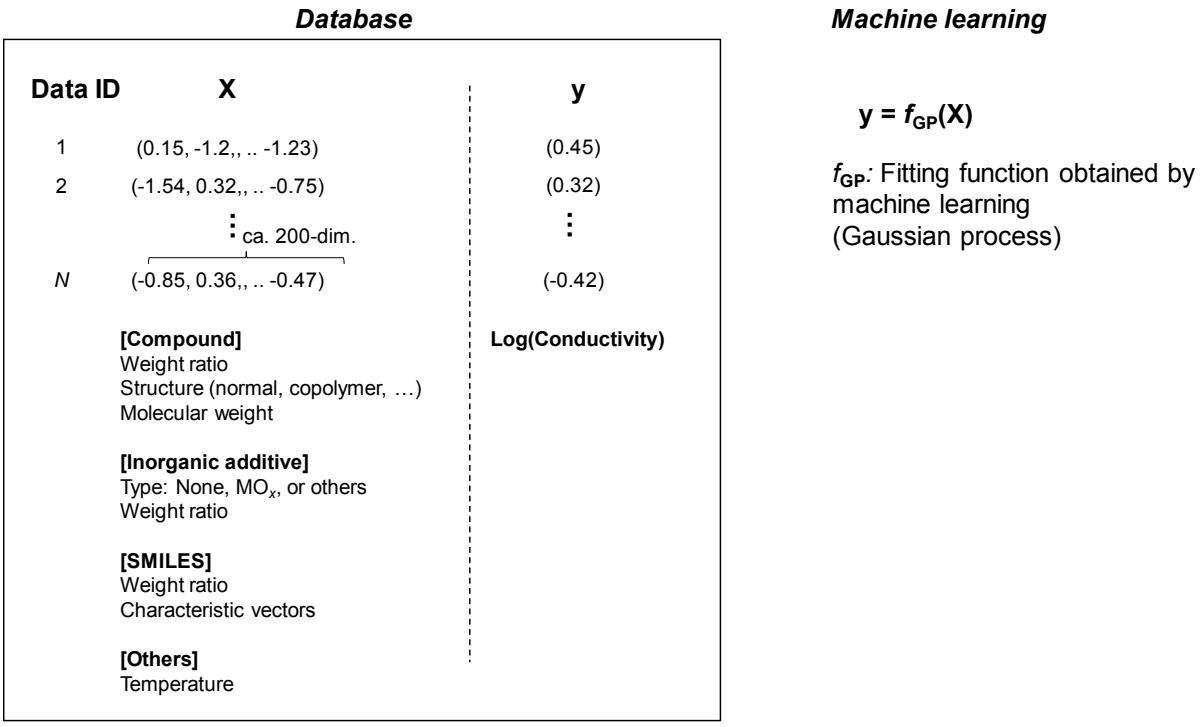

Figure S14. Machine learning of ionic conductivity by Gaussian process.

Pretraining of graph neural network

To calculate the 32-dimensional vectors of chemicals, a graph neural network, pretrained by an *in-silico* chemical database, was constructed.

(1) Preparation of *in-silico* database

Using an original Python script, an *in-silico* database was constructed. Firstly, chemical structures recorded in the compound database (and open chemical databases, ZINC and PubChem) were fragmented into small components (Figure S15). In the figure, the fragmented parts were marked by asterisk symbols. The fragments were connected randomly to yield new, 5×10^4 types of chemical structures. The chemicals were filtered according to the following rules.

[Charge and stability]

The charges of the chemicals were limited to be -1 (anion), 0 (neutral), or 1 (cation). Multivalent ions, such as dianions, were excluded because they were not normally used for Li^+ conductors. Unstable compounds, such as radicals and carboy anions, were also excluded.

[Molecular weight]

Too large molecules, having molecular weights over 400 (per unit), were removed, because those randomly generated, huge structures were too messy and infeasible to be synthesized.

[Bonds for repeating unit]

The number of "Mg" symbols, which stand for the bonds for repeating units, were limited to be zero (*i.e.*, monomeric species) or two (linear polymers).

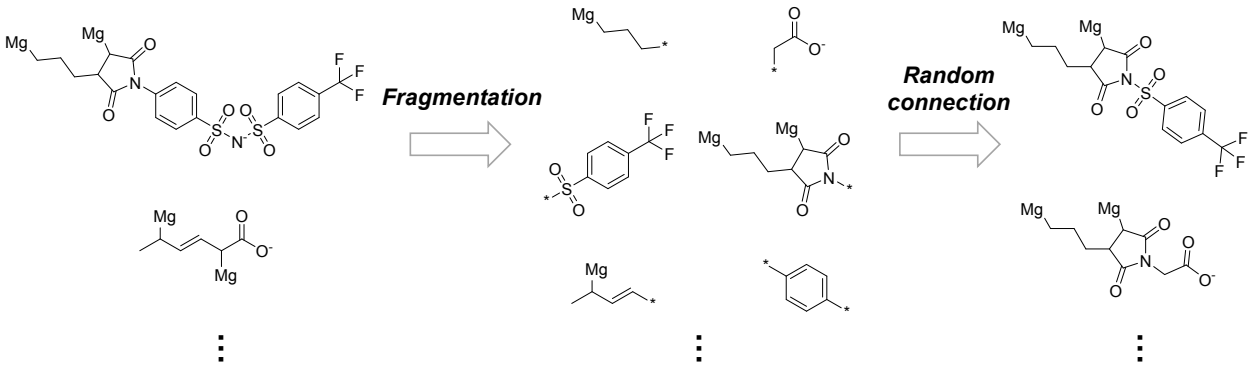

Figure S15. Fragmentation and re-connection of chemicals to generate random molecules.

(2) Machine learning of chemical structures

About 2000 types of molecular descriptors of molecules in the *in-silico* database were calculated using Python modules, Mordred 1.1.1 and RDKit 2018.09.1 The descriptors would cover the most important features to describe the corresponding molecules. Using a neural network (f_{NN}), the relationship between the molecules (X) and their descriptors (Y) were trained (Figure S16). The network was prepared to obtain the characteristic vectors of the molecules, as described later. The configuration of the network is shown in Figure S17.

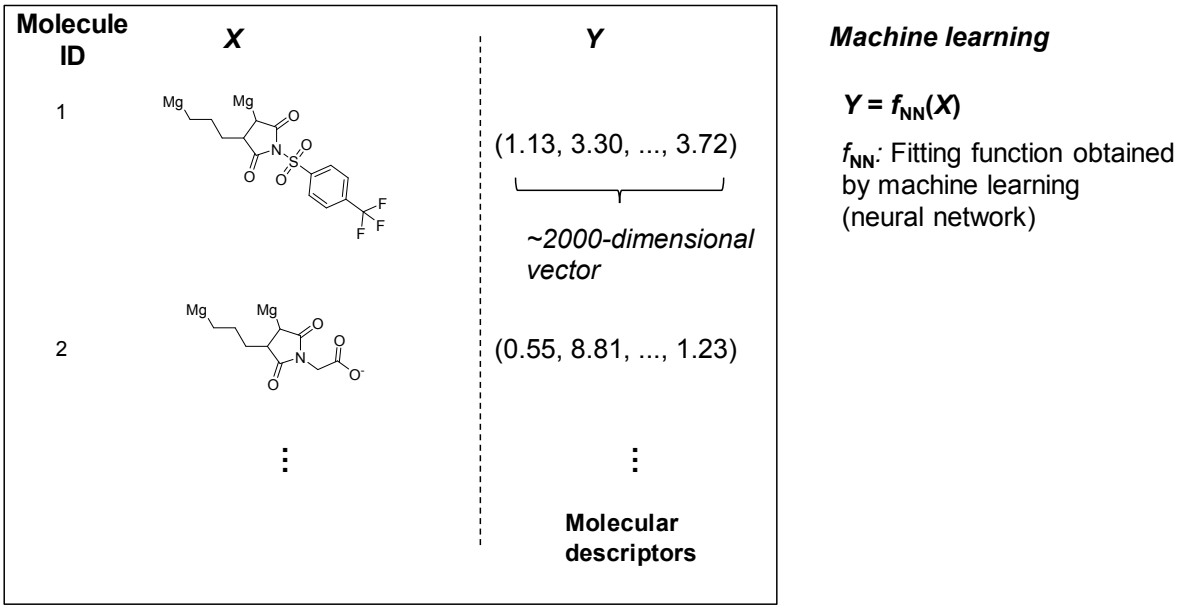

Figure S16. Training the relationship between chemical structures and molecular descriptors.

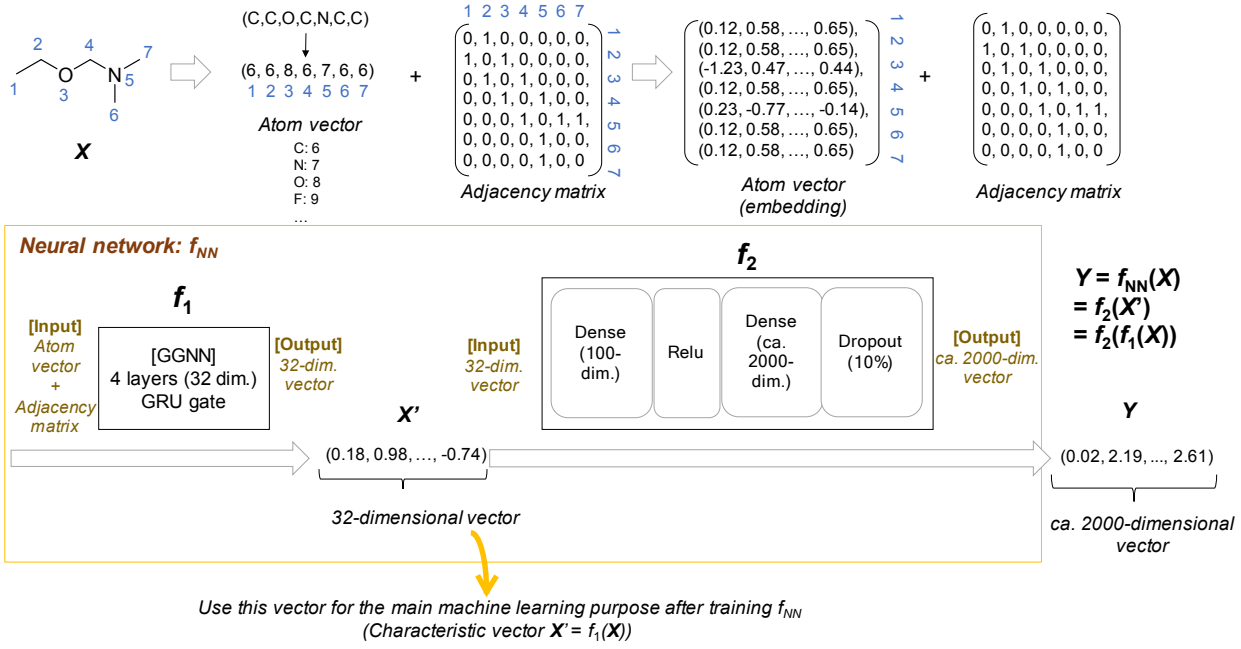

Figure S17. Configuration of the neural network for molecular recognition.

For machine learning, chemical structures were converted to matrix expressions. The conversion was done using an implemented function in an open source library, Chainer Chemistry 0.4.0 (see details on a website https://github.com/pfnet-research/chainer-chemistry). Firstly, unique numbers were allocated to distinguish each atom (marked by blue numbers in the figure). String arrays were generated to express the types of atoms (*e.g.*, (C, C, O, C, N, C, C)). For numeric expression, the atom symbols (C, N, O, …) were replaced by their atomic numbers (6, 7, 8, …). Further, the numbers were converted to 32-dimensional, so-called embedding expression, using "EmbedID" function in Chainer (embedding layers were also trained during machine learning although the process exits out of the neural network in Figure S17). Adjacency matrices M were also made to show the chemical connections. Matrix elements M_{ij} and M_{ji} would be 1 if the atoms, having the unique numbers i and j, were connected (and $M_{ij} = M_{ji} = 0$ if not connected). Additional matrices were generated similarly to express the multiple bonds.

The generated matrices (X) were inputted to a gated graph neural network (GGNN, f_1). In brief, this neural network automatically calculates n-dimensional numeric arrays as the output, from the inputted adjacency matrices and embedding vectors. The implemented neural network function of Chainer Chemistry was used without modification (for further information of the neural network, please check the related references[22-23] and documentation of the library, https://github.com/pfnet-research/chainer-chemistry). The network had four update layers with gated recurrent units (GRUs). 32-Dimenstional vectors (X', arrays of floating-point numbers in Python) were generated as the output of the GGNN.

Another neural network part, f_2, was connected to calculate the fingerprints of the compounds, which were treated as *ca.* 2000-dimensional vectors (Y). The network was a simple connection of a dense layer (100-dimensional output), a rectified linear unit (Relu), a dense layer (*ca.* 2000-

dimensional output), and a dropout (10%) layer. Machine learning was done using an Adam optimizer[24] with a mini-batch size of 64. Randomly selected, 10% of the data were used for validation.

The overall relationship between X and Y was fitted by a neural network f_{NN} ($Y = f_{NN}(X) = f_2(X') = f_2(f_1(X))$, Figure S7). The internal, 32-dimensional vectors, X', could be regarded as the compressed form of both their compound matrices and *ca.* 2000 types of molecular descriptors. Therefore, the trained function f_1 was used in the main machine learning process to calculate the characteristics of the chemical structures in the form of 32-dimensional vectors (X'). The whole process can be considered as a kind of transfer learning.

Preparation of solid polymer electrolytes

PPS was obtained from Sigma-Aldrich (glass transition temperature of about 90 °C).[25] PMPS was synthesized according to our previous report ($M_w = 1.4 \times 10^4$).[26] 2,3-Dichloro-5,6-dicyano-*p*-benzoquinone (DDQ), chloranil and LiTFSI were obtained from Tokyo Chemical Industry Co. Poly(ethylene oxide) (PEO, $M_w = 6 \times 10^5$) was purchased from Sigma-Aldrich. *N*-Propyl-*N*-methylpyrrolidinium bis(fluorosulfonyl)imide (ionic liquid) was obtained from FUJIFILM Wako Chemical Co. Electrodes used for lithium-ion batteries ($LiFePO_4$: LFP cathode and $Li_4Ti_5O_{12}$: LTO anode) were produced by Piotrek Co.

The polymer electrolytes were prepared according to a patent[27] with modification. Experiments were conducted under an argon atmosphere to avoid water and oxygen. The typical procedure is as follows. PMPS, chloranil, and LiTFSI (4.2/1/0.34 molar equivalent ratio) were added into chloroform and stirred until complete dissolution. The mixture was heated at 120 °C to remove the solvent. Further, the mixture was thermally annealed at 300 °C under the melt condition for several minutes to proceed homogeneous doping. PPS-based electrolytes were prepared in a similar

procedure, except for adding solvents (everything mixed under the melt conditions). The electrolytes were stable under ambient conditions, but should be kept under a dry atmosphere to avoid moisture absorption by LiTFSI. For PEO-based electrolytes, PEO (250 mg), LiTFSI (106 mg), and ionic liquid (155 μL, molar ratio of 10/1/0.56) were dissolved in 10 mL acetonitrile. The electrolyte film with a thickness of 20 μm was obtained by removing the solvent.

Measurements of the electrolytes

Thermal properties were recorded by differential scanning calorimetry (Q200 TA instrument). Scanning electron microscopy was conducted by JEOL IT-100LA. X-ray diffraction was measured by Rigaku SmartLab. IR spectra were recorded by Jasco FT/IR-6100 (KBr method). A conventional potentiostat (BAS ALS 660D) was used for the electrochemical measurements. Solartron 1260 Impedance/Gain-Phase Analyzer was employed to record AC impedance spectra. The polymer composite was press-formed to prepare electrode films with a thickness of 0.04 ($\pm$ 0.02) cm. For conductivity analysis by AC impedance (10^6 to 1 Hz, amplitude of 10 mV), the prepared film was measured in conventional solid-state cell equipment. The obtained Nyquist plots were analyzed by equivalent circuits. For instance, an experimental semicircle (Figure S20c) was fitted by a parallel RC circuit to obtain the resistance R of 770 Ω and capacitance C of = 0.39 nF. Ionic conductivity was calculated by 1/(R) × (electrolyte thickness)/(electrolyte area) = 1/(770 Ω) × (0.03 cm)/(0.785 cm^2). The apparent relative permittivity of the region was also calculated: $\varepsilon_r = C/(\text{area}) \times (\text{thickness})/\varepsilon_0 = 12$ (ε_0: vacuum permittivity). The value was basically comparable to those of the matrix polymers and organic compounds,[28-29] supporting the validity of the fitting. This comparison was done to identify the origin of the resistance. If inappropriate semicircles, such as reaction resistances, were fitted wrongly, the value would become too large (>10^3) due to

the much larger capacitances of electric double layers, etc. Constant phase elements were used for some cases where semicircles were too depressed. Li^+ transfer number was estimated by a polarization method.[30] The electrolyte was sandwiched by lithium foils, and current change under a constant voltage (10 mV) was monitored. No practical change in impedance (< 1%) was detected before/after polarization. Lithium-ion batteries were fabricated by stacking a cathode (LFP, 1.5 mAh/cm^2), an electrolyte film, and an anode (LTO, 1.6 mAh/cm^2), respectively. LFP and LTO were selected because of their fast and stable charge/discharge. The fabricated cells were kept overnight at room temperature to improve the contacts at interfaces.

Permittivity analysis

The dielectric properties of the electrolytes were analyzed by a Debye relaxation model of electrode polarization (EP).[31-32] The experimental permittivity was fitted by equation (1).

$$\varepsilon = \varepsilon_R + \frac{\Delta\varepsilon_{\mathrm{EP}}}{1 + i2\pi f\tau_{\mathrm{EP}}} \quad (1)$$

(ε_R: permittivity before EP, $\Delta\varepsilon_{\mathrm{EP}}$: increased permittivity by EP at low frequency, f: frequency, and τ_{EP}: relaxation time of EP).

ε_R, $\Delta\varepsilon_{\mathrm{EP}}$, and τ_{EP} were determined by fitting, to obtain ion mobility (μ) and carrier density (p), according to the following equations.

$$\Delta\varepsilon_{\mathrm{EP}} = \left(\frac{L}{2L_{\mathrm{D}}} - 1\right)\varepsilon_R \quad (2)$$

$$L_{\mathrm{D}} = \frac{1}{q}\left(\frac{\varepsilon_R\varepsilon_0 k_B T}{p}\right)^{1/2} \quad (3)$$

$$\tau_{\mathrm{EP}} = \frac{L\ \varepsilon_R\varepsilon_0}{2L_{\mathrm{D}}q\mu p} \quad (4)$$

(L: electrolyte thickness, L_D: Debye length, q: elementary charge, k_B: Boltzmann constant, and T: temperature).

Temperature dependence of carrier density was fitted by Arrhenius equation $p/p_0 = e^{-E_a/RT}$ (R: gas constant, E_a: activation energy). The maximum density p_0 was calculated from stoichiometry ($p_0 = 6.6 \times 10^{20}$ and 2.7×10^{21} cm^{-3} for PMPS and PEO, respectively, assuming that both cations and anions functioned as carriers).

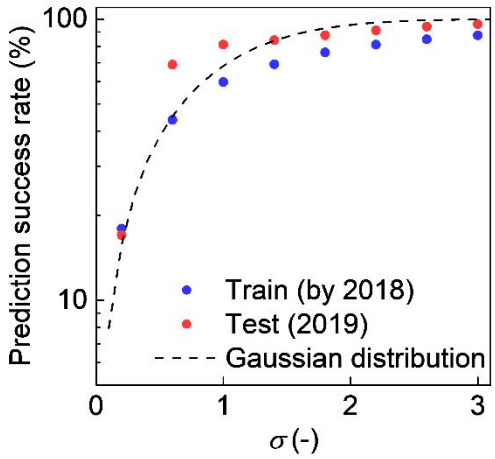

Figure S18. Ratio of samples within the error bars as a function of the confidence interval. The number of the cases whose actual conductivity was within the range of error bars (considered as successful predictions) was counted by changing the confidence intervals in Figure 2a. An ideal curve for a random process (Gaussian distribution) is shown as a dashed line. For the training (samples reported up to 2018) and test datasets (2019), the prediction success rate was explained by the Gaussian curve, meaning that the probabilistic model was valid and treated the uncertainty accurately.

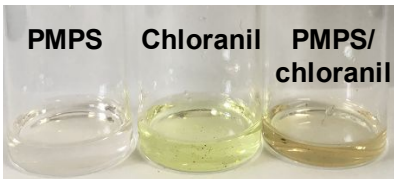

(a)

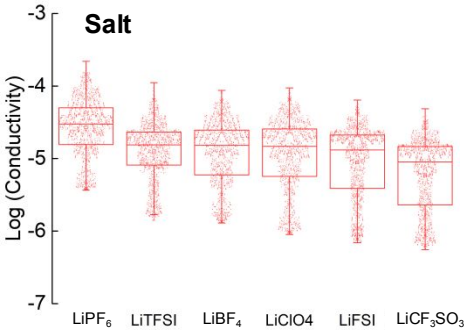

(b)

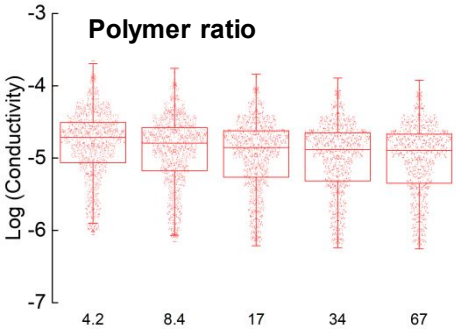

(c)

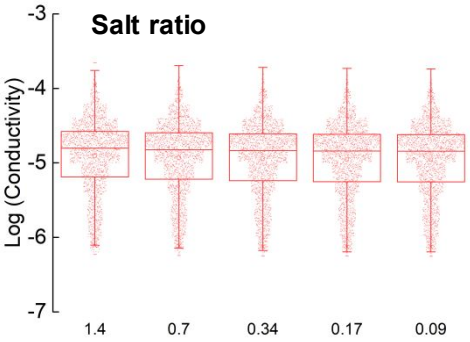

(d)

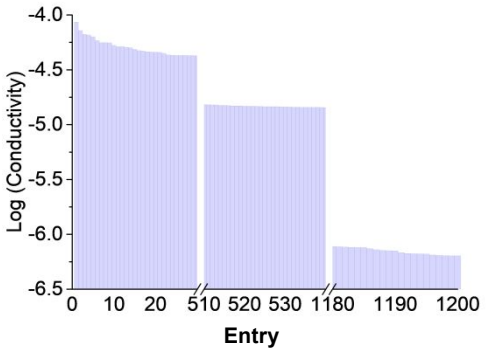

Predicted conductivity (top 30)

Entry	Composition	Mol ratio	Log (Conductivity)
1	2/Chloranil/LiTFSI	4.2/1/1.4	-4.07
2	2/Chloranil/LiTFSI	4.2/1/0.7	-4.14
3	4/Chloranil/LiTFSI	4.2/1/1.4	-4.18
4	2/Chloranil/LiTFSI	8.4/1/1.4	-4.18
5	2/Chloranil/LiTFSI	4.2/1/0.34	-4.20
6	2/Chloranil/LiTFSI	4.2/1/0.17	-4.23
7	2/Chloranil/LiTFSI	4.2/1/0.085	-4.25
8	4/Chloranil/LiTFSI	4.2/1/0.7	-4.25
9	2/Chloranil/LiTFSI	8.4/1/0.7	-4.25
10	2/DDQ/LiTFSI	4.2/1/1.4	-4.28
11	2/Chloranil/LiFSI	4.2/1/1.4	-4.29
12	2/Chloranil/LiTFSI	16.8/1/1.4	-4.29
13	4/Chloranil/LiTFSI	8.4/1/1.4	-4.30
14	2/Chloranil/LiTFSI	8.4/1/0.34	-4.30
15	4/Chloranil/LiTFSI	4.2/1/0.34	-4.31
16	2/Chloranil/LiTFSI	8.4/1/0.17	-4.32
...			
26	2/DDQ/LiFSI	4.2/1/0.7	-4.37
27	2/DDQ/LiTFSI	4.2/1/0.34	-4.37
28	4/Chloranil/LiTFSI	4.2/1/0.085	-4.37
29	4/Chloranil/LiTFSI	8.4/1/0.7	-4.37
30	2/Chloranil/LiTFSI	16.8/1/0.34	-4.37

(e)

Figure S19. Predicted conductivity of charge-transfer complexes. (a) Photograph of the compounds dissolved in chloroform. The brown color of PMPS/chloranil supported the formation

of charge-transfer complex.[33-34] (b), (c), and (d) Box plots to display the predicted effects of electrolyte composition for conductivity. Room temperature conductivity was predicted as a mixture of polymer/dopant/salt = (4.2, 8.4, 17, 34, or 67) /1/ (1.4, 0.7, 0.34, 0.17, or 0.09) (mol/mol/mol). Totally, the conductivity of 9600 (= 8 polymers × 5 molar ratios × 8 dopants × 6 salts × 5 molar ratios) electrolytes were predicted. The conditions with the smaller amount (< 4.2) of polymers and/or the larger amount of salts (> 1.4) were not examined, because insufficient mixtures would be obtained as the electrolytes. (e) Screening process of electrolytes. Initially, a commercially available polymer 4 (PPS) and a highly conducting dimethyl polymer 2 (PMPS) were selected. Polymer 1, exhibiting the highest predicted conductivity, was excluded because it was insoluble to common solvents and difficult to be mixed homogeneously.[35] Several salts ($LiPF_6$, $LiClO_4$, and $LiBF_4$) were also excluded due to the thermal decomposition during annealing (> 200 ^oC).[36] The candidate electrolytes were sorted by predicted conductivity (top 30 are displayed), and several candidates were examined experimentally (highlighted in red).

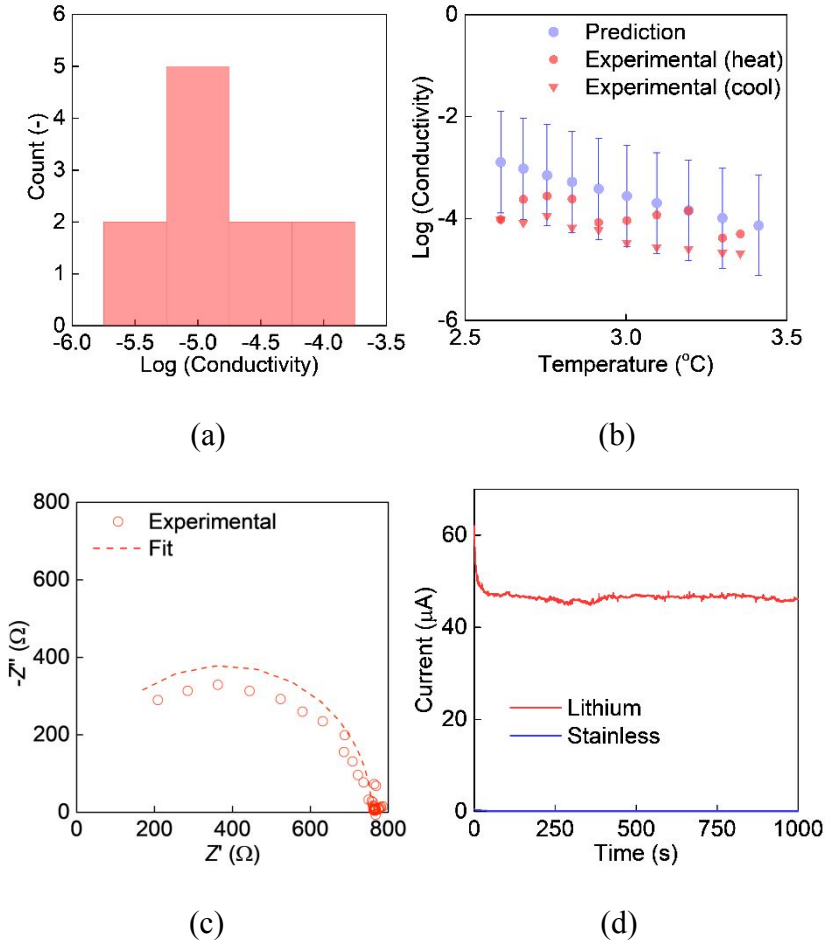

Figure S20. Ionic conductivity of the PMPS/chloranil/LiTFSI (4.2/1/0.34) composite. (a) Histogram of conductivity at room temperature for several samples. Electrolyte preparation procedure should be optimized to decrease the variance of conductivity, which was certainly caused by the slight differences in such as grain boundary. (b) Temperature dependence. Predicted values by AI with 0.5σ error bars are displayed. Experimental conductivity was measured by changing temperatures (heating up to 110 °C, and then cooling down to 25 °C). Fluctuating conductivity during heating was certainly caused by the change of electrolyte interfaces. Activation energy during cooling was analyzed by Arrhenius equation and found to be 20 kJ/mol. (c) Typical Nyquist plot of the electrolyte (the data corresponded to a plot in Figure S20b at 25 °C, before heating). Dashed curve shows the fitting data. (d) Estimation of Li^+ transfer number. The

electrolyte was sandwiched by lithium foils. The calculated transfer number was 0.7, which was consistent with the results of diffusivity measurements by nuclear magnetic resonance (> 0.7).[27] No practical current was detected (< 10^{-7} A) with stainless disks instead of lithium, because the electrolyte was insulating electrons, and stainless was blocking ions. Similar results were obtained with the other compositions.

Table S1. Comparison with representative solid polymer electrolytes with high Li^+ transference number.[1]

No.	Structure[a)]	Log (Conductivity)[b)]	Glass transition temperature (^oC)	Li^+ transference number	Reference
1	PPS or PMPS /chloranil/LiTFSI	-6 to -3	>> r.t.	> 0.7	(this work)
2	LiPPI blend	-5	-40	0.71	[37]
3	LiPSTFSI blend	-9	-	0.92	[38]
4	PSsTFSI blend	-8	-15	0.91	[39]
5	LiPSTFSI-*co*-PEO	-5 (60 ^oC)	-25	0.85	[40]
6	PolyMOB	-5	-52	-	[41]
7	PAN or PDMAA/LiTFSI	< -8	45-50	-	[42]
8	PVICOX/$LiCF_3SO_3$	-4[c)]	-[d)]	-	[43]

[a)]LiPPI: poly(5-oxo-3-oxy-4-trifluoromethyl-1,2,4-pentafluoropentylene sulfonylimide lithium), LiPSTFSI: poly[(4-styrenesulfonyl) (trifluoromethanesulfonyl)imide], PSsTFSI: poly[(4-styrenesulfonyl)(trifluoromethyl(S-trifluoromethylsulfonylimino)sulfonyl)imide], PEO: polyethylene oxide, PolyMOB: Poly(mono-diacyl-capped orthoborate), PAN: poly(acrylonitrile), PDMAA: poly(*N*,*N*-dimethyl arylamide), PVICOX: poly((1,3-dioxolan-2-one-4,5-diyloxalate). [b)]Conductivity at room temperature. [c)]Trace amounts of solvents, contributing to higher conductivity, might be involved in the electrolytes.[42] [d)]No glass transition temperature detected. Melting point of around 100 ^oC.

Table S2. Chemical and physical characteristics of the proposed electrolytes in comparison with the conventional PEO electrolytes.

Feature	PPS or PMPS /chloranil or DDQ /LiTFSI	PEO/ lithium salt (for comparison)
Glass transition temperature	>> r.t.	<< r.t.
Polymer chains	Rigid aromatic thioether	Flexible aliphatic ether
Main functional groups	-S-, benzene ring, >C=O	$-CH_2-O-$
Polarization of the polymer	Stronger (charge transfer complex)	Weaker (neutral polymer)
Phase	Amorphous (PMPS) or Amorphous + crystalline (PPS)	Amorphous + crystalline (PEO)
Microscopic homogeneity	Contain grain boundaries (see Figure S21)	Basically homogeneous
Ion conduction	Probably decoupled from the segmental motion of polymer chains	By the segmental motion of polymer chains

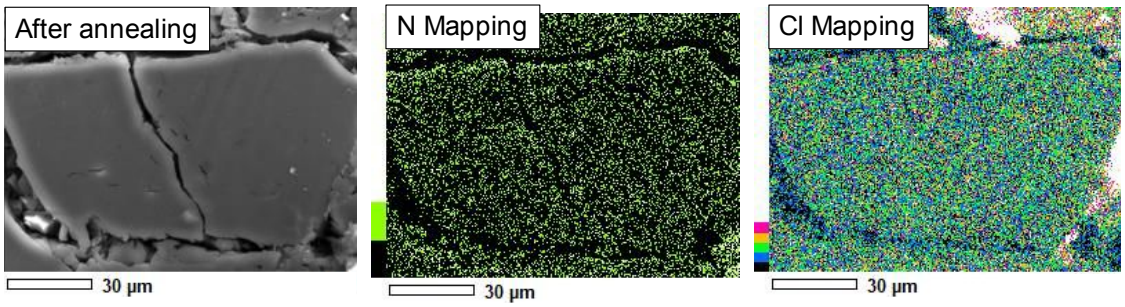

(a)

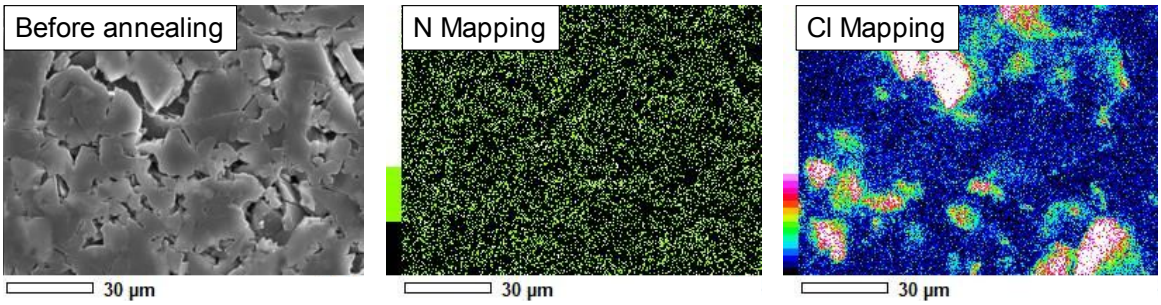

(b)

Figure S21. Scanning electron microscope images of the PMPS/chloranil/LiTFSI (4.2/1/0.34) composite. (a) After annealing at 300 °C and (b) before annealing. Homogeneous dispersion of LiTFSI was observed before/after thermal annealing, as indicated by nitrogen mapping. In contrast, additional thermal treatment was necessary to dope the polymer homogeneously by chloranil (Cl mapping).

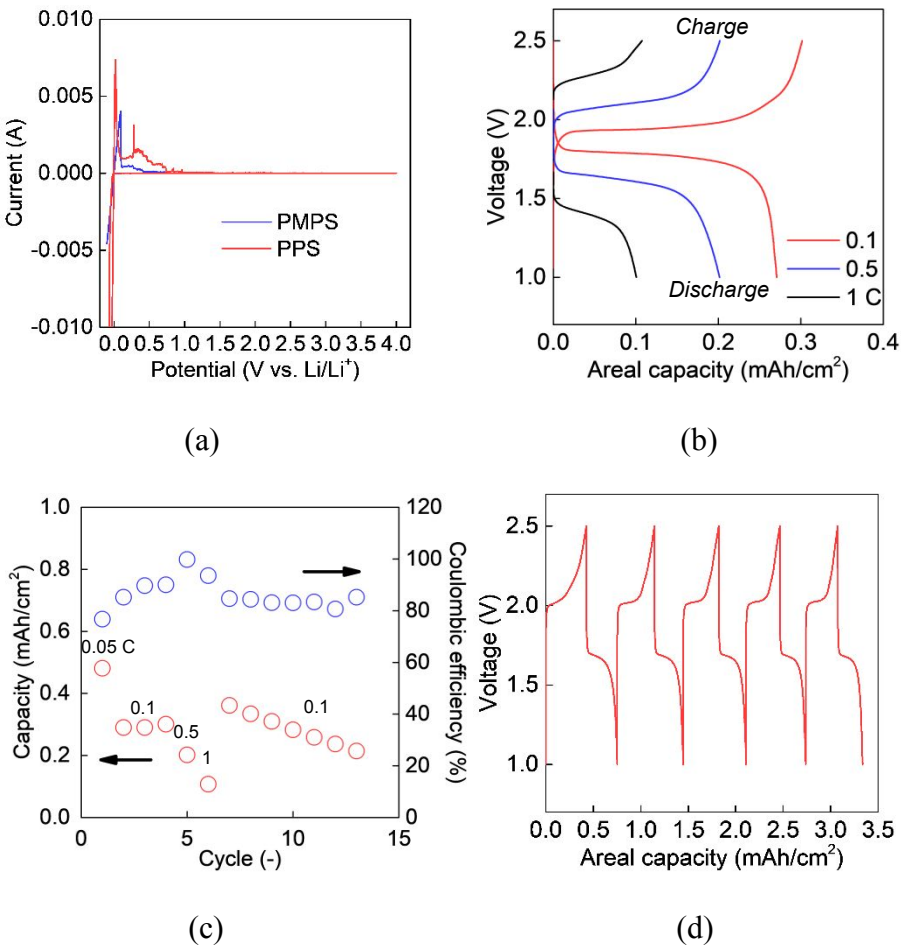

Figure S22. Electrochemical properties of the polymer/chloranil/LiTFSI composites. (a) Potential window (cyclic voltammogram scanned at 10 mV/s). The electrolyte film (molar ratio of 4.2/1/0.34) was sandwiched by a lithium foil and a stainless disk. The oxidation/reduction waves around 0 V were attributed to the redox of lithium. (b) Typical charge/discharge curves of a prototype lithium-ion battery with a PPS/chloranil/LiTFSI (4.2/1/1.4) electrolyte. The formal areal electrode capacity was 1.5 mAh/cm^2. The cell configuration should be optimized for higher experimental capacity (*e.g.*, improve interface contact). (c) Cycle performance (0.05, 0.1, 1, and 0.1 C). (d) Charge/discharge curves for a cell with a PMPS/chloranil/LiTFSI (4.2/1/1.4) electrolyte (0.2 C). Although no significant side-reaction peaks or plateaus were detected, redox reactions by chloranil[44] may have affected the attenuation of charge/discharge capacity. The issue will be

solved by optimizing the cell configuration, such as inserting electrochemically stable layers between the electrolytes and electrode materials.[45]

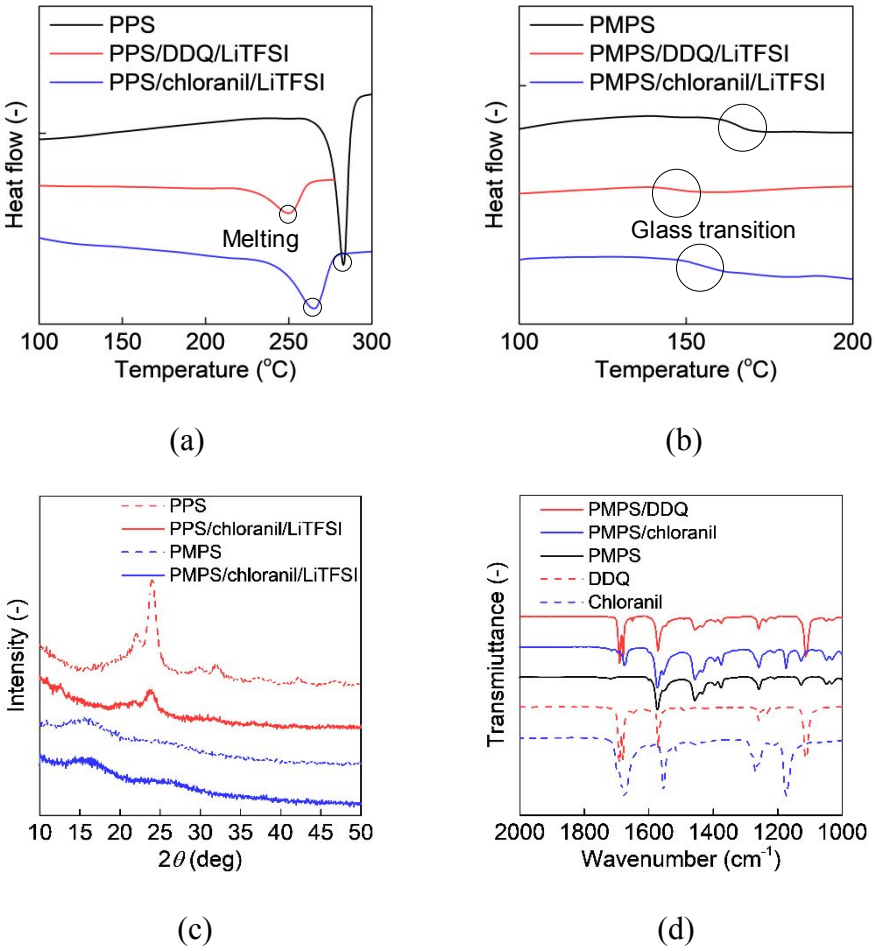

Figure S23. Thermal and crystallographic properties of the polymer electrolytes. (a) and (b) Differential scanning calorimetry for the polymer composites (polymer/dopant/LiTFSI = 4.2/1/0.34), scanned at 20 °C/min. Glass transition temperature for PMPS/chloranil/LiTFSI (4.2/1/1.4) was around 130 °C. The melting point for PPS/chloranil/LiTFSI (4.2/1/1.4) was about 270 °C. (c) X-ray diffraction spectra. Amorphous polymer PMPS did not exhibit any diffraction peaks by crystalline structures, in contrast to PPS. Since no practical glass transition temperature was detected for the PPS composites, the value for a pristine PPS was used to plot data in Figure2.

(d) IR spectra. To obtain clearer spectra, samples were prepared without LiTFSI. No significant peak shift or evolution was detected even after the composition, suggesting the absence of side reactions such as sulfoxide or sulfone formation.

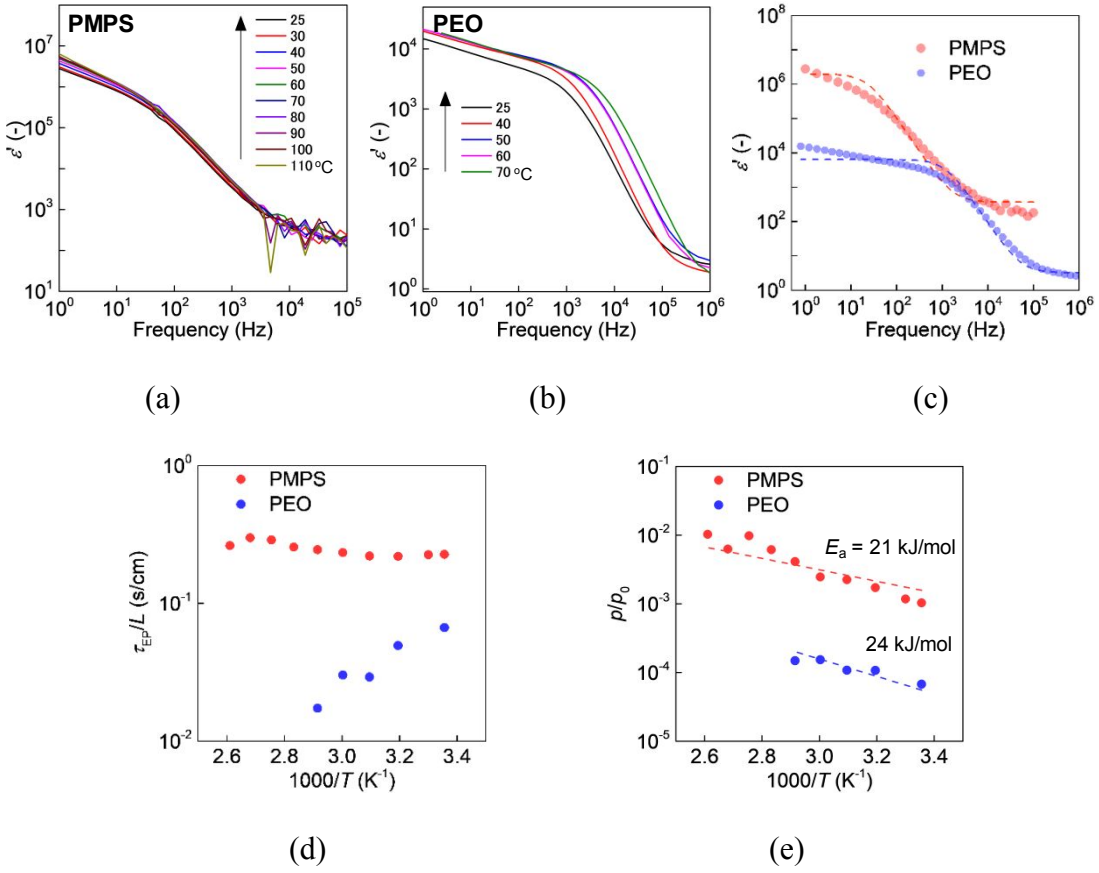

Figure S24. Dielectric properties of the PMPS (4.2/1/0.34) composite and PEO-based electrolytes. (a) and (b) frequency and temperature dependence of dielectric constant. (c) Typical fitting results for permittivity. In the graph, experimental plots at room temperature were fitted by equation (1) (dashed lines). (d) Relaxation time of electrode polarization (τ_{EP}) as a function of temperature. The value was normalized by the electrolyte thickness (L). In the case of the PEO-based electrolyte, τ_{EP} decreased by elevating temperature, because of the more activated segmental motion of the polymer chains.[32] In contrast, the invariance of τ_{EP} with PMPS indicated the decoupled motion of

ionic species from the polymer matrix. (e) Carrier density. The temperature dependence of carrier ratio p/p_0 was analyzed by Arrhenius equation.

References

(1) Zhang, H.; Li, C.; Piszcz, M.; Coya, E.; Rojo, T.; Rodriguez-Martinez, L. M.; Armand, M.; Zhou, Z., Single lithium-ion conducting solid polymer electrolytes: advances and perspectives. *Chem. Soc. Rev.* **2017,** *46*, 797-815.

(2) Yue, L.; Ma, J.; Zhang, J.; Zhao, J.; Dong, S.; Liu, Z.; Cui, G.; Chen, L., All solid-state polymer electrolytes for high-performance lithium ion batteries. *Energy Storage Materials* **2016,** *5*, 139-164.

(3) Yu, Y.; Lu, F.; Sun, N.; Wu, A.; Pan, W.; Zheng, L., Single lithium-ion polymer electrolytes based on poly(ionic liquid)s for lithium-ion batteries. *Soft Matter* **2018,** *14*, 6313-6319.

(4) Long, L. Z.; Wang, S. J.; Xiao, M.; Meng, Y. Z., Polymer electrolytes for lithium polymer batteries. *J. Mater. Chem. A* **2016,** *4*, 10038-10069.

(5) Jow, T. R.; Xu, K.; Borodin, O.; Ue, M., *Electrolytes for Lithium and Lithium-Ion Batteries*. Springer-Verlag New York: 2014.

(6) Dudley, J. T.; Wilkinson, D. P.; Thomas, G.; LeVae, R.; Woo, S.; Blom, H.; Horvath, C.; Juzkow, M. W.; Denis, B.; Juric, P.; Aghakian, P.; Dahn, J. R., Conductivity of electrolytes for rechargeable lithium batteries. *J. Power Sources* **1991,** *35*, 59-82.

(7) Lin, T. S.; Coley, C. W.; Mochigase, H.; Beech, H. K.; Wang, W.; Wang, Z.; Woods, E.; Craig, S. L.; Johnson, J. A.; Kalow, J. A.; Jensen, K. F.; Olsen, B. D., BigSMILES: A Structurally-Based Line Notation for Describing Macromolecules. *ACS Cent. Sci.* **2019,** *5*, 1523-1531.

(8) Mindemark, J.; Lacey, M. J.; Bowden, T.; Brandell, D., Beyond PEO—Alternative host materials for Li + -conducting solid polymer electrolytes. *Prog. Polym. Sci.* **2018,** *81*, 114-143.

(9) Hatakeyama-Sato, K.; Tezuka, T.; Nishikitani, Y.; Nishide, H.; Oyaizu, K., Synthesis of Lithium-ion Conducting Polymers Designed by Machine Learning-based Prediction and Screening. *Chem. Lett.* **2019,** *48*, 130-132.

(10) Nag, A.; Ali, M. A.; Singh, A.; Vedarajan, R.; Matsumi, N.; Kaneko, T., N-Boronated polybenzimidazole for composite electrolyte design of highly ion conducting pseudo solid-state ion gel electrolytes with a high Li-transference number. *J. Mater. Chem. A* **2019,** *7*, 4459-4468.

(11) Yang, K. H.; Liao, Z.; Zhang, Z. X.; Yang, L.; Hirano, S., Ionic plastic crystal-polymeric ionic liquid solid-state electrolytes with high ionic conductivity for lithium ion batteries. *Mater. Lett.* **2019,** *236*, 554-557.

(12) Huang, S.; Cui, Z.; Qiao, L.; Xu, G.; Zhang, J.; Tang, K.; Liu, X.; Wang, Q.; Zhou, X.; Zhang, B.; Cui, G., An in-situ polymerized solid polymer electrolyte enables excellent interfacial compatibility in lithium batteries. *Electrochim. Acta* **2019,** *299*, 820-827.

(13) Zhang, H.; Oteo, U.; Zhu, H.; Judez, X.; Martinez-Ibanez, M.; Aldalur, I.; Sanchez-Diez, E.; Li, C.; Carrasco, J.; Forsyth, M.; Armand, M., Enhanced Lithium-Ion Conductivity of Polymer

Electrolytes by Selective Introduction of Hydrogen into the Anion. *Angew. Chem. Int. Ed.* **2019**.
(14) Eriksson, T.; Mindemark, J.; Yue, M.; Brandell, D., Effects of nanoparticle addition to poly(ε-caprolactone) electrolytes: Crystallinity, conductivity and ambient temperature battery cycling. *Electrochim. Acta* **2019,** *300*, 489-496.
(15) Li, X.; Wang, Z. J.; Lin, H.; Liu, Y. D.; Min, Y.; Pan, F., Composite electrolytes of pyrrolidone-derivatives-PEO enable to enhance performance of all solid state lithium-ion batteries. *Electrochim. Acta* **2019,** *293*, 25-29.
(16) Longstaff, M.; Gardiner, K.; Zhuravlev, R.; Finney, J.; Waldow, D. A., Characterization of morphology in ring-opening metathesis polymerized novel solid block copolymer electrolytes by atomic force microscopy and X-ray scattering. *Electrochim. Acta* **2019,** *298*, 339-346.
(17) Moriwaki, H.; Tian, Y. S.; Kawashita, N.; Takagi, T., Mordred: a molecular descriptor calculator. *J. Cheminform.* **2018,** *10*, 4.
(18) Ramprasad, R.; Batra, R.; Pilania, G.; Mannodi-Kanakkithodi, A.; Kim, C., Machine learning in materials informatics: recent applications and prospects. *Npj Comput. Mater.* **2017,** *3*, 54.
(19) Ruddigkeit, L.; van Deursen, R.; Blum, L. C.; Reymond, J. L., Enumeration of 166 billion organic small molecules in the chemical universe database GDB-17. *J. Chem. Inf. Model.* **2012,** *52*, 2864-75.
(20) Butler, K. T.; Davies, D. W.; Cartwright, H.; Isayev, O.; Walsh, A., Machine learning for molecular and materials science. *Nature* **2018,** *559*, 547-555.
(21) McInnes, L.; Healy, J.; Melville, J., UMAP: Uniform Manifold Approximation and Projection for Dimension Reduction. **2018**.
(22) Gilmer, J.; Schoenholz, S.; Riley, P.; Vinyals, O.; Dahl, G., Neural Message Passing for Quantum Chemistry. *arXiv:1704.01212v2* **2017**.
(23) Li, Y.; Tarlow, D.; Brockschmidt, M.; Zemel, R., Gated Graph Sequence Neural Networks. *arXiv:1511.05493* **2017**.
(24) Kingma, D. P.; Ba, J., Adam: A Method for Stochastic Optimization. **2014**.
(25) Cheng, S. Z. D.; Wu, Z. Q.; Wunderlich, B., Glass-Transition and Melting Behavior of Poly(Thio-1,4-Phenylene). *Macromolecules* **1987,** *20*, 2802-2810.
(26) Jikei, M.; Katoh, J.; Sato, N.; Yamamoto, K.; Nishide, H.; Tsuchida, E., Synthesis of Soluble Poly(Thio-2,6-Dimethyl-1,4-Phenylene) by Oxidative Polymerization of Bis(3,5-Dimethylphenyl) Disulfide. *Bull. Chem. Soc. Jpn.* **1992,** *65*, 2029-2036.
(27) Zimmerman, M., Solid ionically conducting polymer material. **2016**, USA patent 15/282002.
(28) Hikosaka, S.; Ohki, Y., Dielectric properties of poly(phenylene sulfide) as a function of temperature and frequency. *Ieej Transactions on Electrical and Electronic Engineering* **2012,** *7*, 116-120.
(29) Sidletskiy, O. T.; Lisetski, L. N.; Malikov, V. Y.; Stadnik, P. E.; Panikarskaya, V. D.; Budakovsky, S. V., Dielectric and spectral studies of molecular crystal-chloranil systems forming charge transfer complexes. *Molecular Crystals and Liquid Crystals* **2002,** *384*, 101-109.
(30) Zugmann, S.; Fleischmann, M.; Amereller, M.; Gschwind, R. M.; Wiemhofer, H. D.; Gores, H. J., Measurement of transference numbers for lithium ion electrolytes via four different methods, a comparative study. *Electrochim. Acta* **2011,** *56*, 3926-3933.
(31) Klein, R. J.; Zhang, S.; Dou, S.; Jones, B. H.; Colby, R. H.; Runt, J., Modeling electrode polarization in dielectric spectroscopy: Ion mobility and mobile ion concentration of single-ion polymer electrolytes. *J. Chem. Phys.* **2006,** *124*, 144903.

(32) Fragiadakis, D.; Dou, S.; Colby, R. H.; Runt, J., Molecular Mobility, Ion Mobility, and Mobile Ion Concentration in Poly(ethylene oxide)-Based Polyurethane Ionomers. *Macromolecules* **2008,** *41*, 5723-5728.
(33) Tsutsui, T.; Nitta, N.; Saito, S., Electronic conduction in poly(p‐phenylene sulfide). *J. Appl. Phys.* **1985,** *57*, 5367-5371.
(34) Tokito, S.; Tsutsui, T.; Saito, S., Electrical Conductivity and Optical Properties of Poly(p-phenylene sulflde) Doped with Some Organic Acceptors. *Polym. J.* **1985,** *17*, 959-968.
(35) Tsuchida, E.; Miyatake, K.; Yamamoto, K.; Hay, A. S., Cyclic arylene sulfides: A novel synthesis and ring-opening polymerization. *Macromolecules* **1998,** *31*, 6469-6475.
(36) Ping, P.; Wang, Q.; Sun, J.; Xiang, H.; Chen, C., Thermal Stabilities of Some Lithium Salts and Their Electrolyte Solutions With and Without Contact to a LiFePO[sub 4] Electrode. *J. Electrochem. Soc.* **2010,** *157*.
(37) Watanabe, M.; Tokuda, H.; Muto, S., Anionic effect on ion transport properties in network polyether electrolytes. *Electrochim. Acta* **2001,** *46*, 1487-1491.
(38) Feng, S. W.; Shi, D. Y.; Liu, F.; Zheng, L. P.; Nie, J.; Feng, W. F.; Huang, X. J.; Armand, M.; Zhou, Z. B., Single lithium-ion conducting polymer electrolytes based on poly[(4-styrenesulfonyl)(trifluoromethanesulfonyl)imide] anions. *Electrochim. Acta* **2013,** *93*, 254-263.
(39) Ma, Q.; Zhang, H.; Zhou, C.; Zheng, L.; Cheng, P.; Nie, J.; Feng, W.; Hu, Y. S.; Li, H.; Huang, X.; Chen, L.; Armand, M.; Zhou, Z., Single Lithium-Ion Conducting Polymer Electrolytes Based on a Super-Delocalized Polyanion. *Angew. Chem. Int. Ed.* **2016,** *55*, 2521-5.
(40) Bouchet, R.; Maria, S.; Meziane, R.; Aboulaich, A.; Lienafa, L.; Bonnet, J. P.; Phan, T. N.; Bertin, D.; Gigmes, D.; Devaux, D.; Denoyel, R.; Armand, M., Single-ion BAB triblock copolymers as highly efficient electrolytes for lithium-metal batteries. *Nat Mater* **2013,** *12*, 452-7.
(41) Xu, W.; Williams, M. D.; Angell, C. A., Novel polyanionic solid electrolytes with weak Coulomb traps and controllable caps and spacers. *Chem. Mater.* **2002,** *14*, 401-409.
(42) Forsyth, M.; Jiazeng, S.; MacFarlane, D. R., Novel high salt content polymer electrolytes based on high Tg polymers. *Electrochim. Acta* **2000,** *45*, 1249-1254.
(43) Wei, X.; Shriver, D. F., Highly Conductive Polymer Electrolytes Containing Rigid Polymers. *Chem. Mater.* **1998,** *10*, 2307-2308.
(44) Schon, T. B.; McAllister, B. T.; Li, P. F.; Seferos, D. S., The rise of organic electrode materials for energy storage. *Chem. Soc. Rev.* **2016,** *45*, 6345-6404.
(45) Zhou, W.; Wang, S.; Li, Y.; Xin, S.; Manthiram, A.; Goodenough, J. B., Plating a Dendrite-Free Lithium Anode with a Polymer/Ceramic/Polymer Sandwich Electrolyte. *J. Am. Chem. Soc.* **2016,** *138*, 9385-8.